3-8-2004

Characterization of Ultra Wideband Multiple Access Performance Using Time Hopped-Biorthogonal Pulse Position Modulation

Donald J. Clabaugh

AFIT/GE/ENG/04-03

CHARACTERIZATION OF ULTRA WIDEBAND MULTIPLE ACCESS PERFORMANCE USING TIME HOPPED-BIORTHOGONAL PULSE POSITION MODULATION

THESIS

Donald J. Clabaugh
Chief Master Sergeant, USAF

AFIT/GE/ENG/04-03

DEPARTMENT OF THE AIR FORCE

AIR UNIVERSITY

AIR FORCE INSTITUTE OF TECHNOLOGY

Wright-Patterson Air Force Base, Ohio

The views expressed in this thesis are those of the author and do not reflect the official policy or position of the United States Air Force, Department of Defense, or the United States Government.

AFIT/GE/ENG/04-03

CHARACTERIZATION OF ULTRA WIDEBAND MULTIPLE ACCESS PERFORMANCE USING TIME HOPPED-BIORTHOGONAL PULSE POSITION MODULATION

THESIS

Presented to the Faculty

Department of Electrical and Computer Engineering

Graduate School of Engineering and Management

Air Force Institute of Technology

Air University

Air Education and Training Command

In Partial Fulfillment of the Requirements for the

Degree of Master of Science in Electrical Engineering

Donald J. Clabaugh, B.S.E.

Chief Master Sergeant, USAF

March 2004

AFIT/GE/ENG/04-03

CHARACTERIZATION OF ULTRA WIDEBAND MULTIPLE ACCESS PERFORMANCE USING TIME HOPPED-BIORTHOGONAL PULSE POSITION MODULATION

THESIS

Donald J. Clabaugh, B.S.E.

Chief Master Sergeant, USAF

Approved:

/signed/	8 Mar 04
Dr. Michael A. Temple Thesis Advisor	Date
/signed/	8 Mar 04
Dr. Richard A. Raines Committee Member	Date
/signed/	8 Mar 04
Major Rusty O. Baldwin Committee Member	Date

Acknowledgements

I'm thrilled and amazed to be writing an acknowledgement page to an Air Force Institute of Technology Master's thesis. Just when I felt my formal education was complete, the Air Force opened another door to the enlisted force. MSgt Horace Booker had the fortitude to question Secretary Roche who in turn had the mettle to make a change. Never in my career was the Air Force culture more fertile for change and supportive of education or the enlisted force. From the time the question was asked, to the time SMSgt Szabo, SMSgt Carroll, MSgt Sorgaard, MSgt Kuntzelman, MSgt Swayne, MSgt Mathews, MSgt Cruz, and I set foot in the hallways of AFIT was a mere six months. To be honest, the process may not have moved so quickly were it not for the fact that six enlisted Marines had already gained approval for attendance in the fall of 2002, but whatever the motivation, it took the commitment, support, and direction of Secretary Roche, General Jumper, and CMSAF Murray to make it a reality. The daunting task of transforming me into a Communication Engineer fell firmly on the shoulders of Dr. Temple, my advisor. He, along with Jim Stephens, my Air Force Research Lab sponsor, led me down a path of research success and proved you can teach an old dog new tricks. Lastly, I'd be remiss if I forgot "my" young Lieutenants–I traded my experience for their fresh minds.

The Air Force may have provided the opportunity, but it would have been an opportunity missed without the love and support of my lovely bride of 21 years and the understanding of my daughter. Though I may have struggled through the course work, they sacrificed in order for me to reach my goal and for that I owe them immensely.

To paraphrase one of my heroes, I feel Neil Armstong would sum it up by saying "This is one small step for eight enlisted, one giant leap for the enlisted force."

Donald J. Clabaugh

Table of Contents

List of Figures

List of Tables

Abstract

The FCC's release of its UWB First Report and Order in April 2002 spawned renewed interest in impulse signaling research. This work combines Time Hopped (TH) multiple access coding with 4-ary UWB biorthogonal Pulse Position Modulation (TH-BPPM). Multiple access performance is evaluated in a multipath environment for both synchronous and asynchronous networks. Fast time hopping is implemented by replicating and hopping each TH-BPPM symbol N_H times. Bit error expressions are derived for biorthogonal TH-BPPM signaling and results compared with previous orthogonal TH-PPM work. Without fast time hopping ($N_H = 1$), the biorthogonal TH-BPPM technique provided gains equivalent to Gray-coded QPSK; improved BER at a given E_b/N_o and an effective doubling of the data rate. A synchronized network containing up to $N_T = 15$ transmitters yields an average *BER improvement* (relative to an asynchronous network) of approximately -6.30 dB with orthogonal TH-PPM and approximately -5.9 dB with biorthogonal TH-BPPM. Simulation results indicate that doubling the number of multipath replications (N_{MP}) reduces BER by approximately 3.6 dB. Network performance degrades as N_T and N_{MP} increase and synchronized network advantages apparent in the $N_{MP} = 0$ case diminish with multipath interference present. Fast time hopping (N_H>1) improves BER performance whenever N_{MP}<N_H while reducing effective data rate by $1/N_H$. Compared to the $N_H = 1$ synchronized network, TH-BPPM modulation using $N_H = 10$ provides approximately -5.9 dB improvement at $N_{MP} = 0$ and approximately -3.6 dB improvement at $N_{MP} = 5$. At $N_{MP} = 10$, the BER for the hopped and $N_H = 1$ cases are not statistically different; with $N_H = 10$ hops, *BER improvement* varies from approximately -0.57 to 0.14 dB (minimal variation between synchronous and asynchronous network performance).

CHARACTERIZATION OF ULTRA WIDEBAND MULTIPLE ACCESS PERFORMANCE USING TIME HOPPED-BIORTHOGONAL PULSE POSITION MODULATION

I. Introduction

1.1 Ultrawideband-An old technology with a new twist

Although Ultrawideband (UWB) technology was first introduced in the mid-1960s, it wasn't until the digital age of the late 1980s and 1990s that realistic implementation was possible. UWB gained a great deal of attention over the last decade as civilian and military research communities developed applications for the technology. Recent approval by the Federal Communications Commission (FCC) [1] opened the doorway to fielding particular applications. The UWB signal structure makes it well-suited for use in communications, vehicular radar, and ground penetrating radar. It has also gained a considerable following among the special operations and radar communities because of its low probability of intercept and detection, multipath immunity, high data throughput, and precision ranging and localization.

Prior to the FCC's release of its First Report and Order [1], UWB communication systems research focused on two dominant modulation schemes, direct sequence-binary phase shift key (DS-BPSK) and time hopped-pulse position modulation (TH-PPM). This was due mainly to the limited market and FCC restrictions. Though introduced as a hybrid modulation scheme [2], very little research has been conducted on m-ary systems and even less on biorthogonal signaling. This work extends the body of knowledge in both these areas.

1.2 Beneficial Characteristics

The spectral characteristics inherent to a nanosecond burst (UWB pulse) are of keen interest to military researchers studying radar fading, radar cross section (RCS), and low probability of intercept/detection.

Narrowband detection of UWB signal fluctuates slowly without multiple peaks or deep nulls. Rapid multiple fades and radar scintillation typical of narrowband communication and radar systems are largely mitigated with UWB since the multiple lobes are effectively eliminated. Tracking multiple responses and applying rake processing is easier with UWB modulation due to reduced scintillation and fluctuation rates. For example, most synthetic aperture radar (SAR) images, contain speckle. Speckle is an interference pattern caused by multiple time shifted waves that are incoherently detected. UWB SAR images contain no speckle because the sum of single-cycle waveforms sliding in time with respect to one another never sum *destructively* to create multiple nulls or *constructively* to create peaks, unless they are exactly aligned [3].

For the RCS engineer, the multi-gigahertz frequency spectrum of UWB radars is advantageous when used to identify scattering mechanisms; the ratio of object physical size to electrical wavelength governs object scattering characteristics and return signal strength is typically proportional to the frequency. When the electrical wavelength is large compared to the object's physical dimensions, the target's RCS is determined more by the scatterer's volume than by its shape; when the wavelength is small with respect to the target, i.e., the optical scattering region, target shape influences the RCS the greatest. In the resonant scattering region, the wavelength is comparable to the target dimensions [4]. These regions are important for radar and communications because as frequency decreases, scattering lobes become broader and objects scatter less or stop scattering. For the radar, this phenomenon reduces clutter. With respect to communication systems, this phenomenon reduces the den-

sity of multipath reflections and multipath variance due to the broader scattering lobes [3].

The UWB transmission system's large bandwidth is fundamentally a function of the generated pulse shape and duration. The system bandwidth relative to the information bandwidth allows UWB systems to operate with a low power spectral density. A low power spectral density would seem to indicate an inherent covertness of UWB given that the UWB signal may be near or below the noise floor of a hostile detection device [5]. Thus, UWB is highly useful for military applications requiring covert communication in hostile environments while the wide spectrum makes it relatively insensitive to intentional jamming. These characteristics alone warrant investigation of UWB as a next generation communication system for America's warfighters.

1.3 Applications of UWB Technology

The Defense Advanced Research Projects Agency (DARPA) and the Office of the Secretary of Defense (OSD) funded a study panel to examine the potential performance benefits and limitations of UWB technology. DARPA contracted with Batelle to evaluate the use of UWB in radar, communications, electronic warfare, and radio frequency weaponization. The results [6] were published in 1990 and many of the findings drove research over the last decade. Although the panel recommended against Department of Defense (DoD) investment in certain applications, research continued. The 2002 release of [1] provided additional direction while providing a market for previously developed UWB applications. Commercial developers who were previously reluctant to invest in UWB research and hardware, quickly moved into the UWB fray. The following subsections are a small subset of applications that have garnered interest in the UWB community.

1.3.1 Vehicular Radar. Application of UWB in vehicular radar focuses primarily on collision detection and avoidance. The radar is used to trigger visual alerts to aid the driver and could also be used as another sensor input for airbag restraint and deployment. With the resolution provided by the higher frequencies, application engineers are even looking into distinguishing cars, people, animals, or poles on or near roadways. UWB radar has the capability to sense road conditions (e.g., potholes, dips, bumps, gravel vs. pavement) which in turn can be used to dynamically adjust suspension, braking, and other drive systems.

The Multispectral Corporation demonstrated the use of a C-band UWB backup sensor to detect human and vehicle targets, though not in the prescribed FCC vehicular radar band. Human and pickup truck targets were identified at ranges of 1-50 feet, and 1-200 feet, respectively, at extremely low false alarm rates.

1.3.2 Ground/Wall Penetration. Urban warfare and hardened underground bunkers are critical areas of concern for the DoD and the special operations community in particular. Creating a picture of the combatant's environment is paramount to gaining an advantage over ones enemy. UWB techniques may provide the needed enhancements for tomorrow's counterinsurgency operatives. UWB exploitation is not limited to military demands; geophysical surveying and subsurface mapping in mining, agriculture, highway and building construction, archeology, and ice field surveying are one of three development areas allowed by [1].

The penetration depth into a lossy material/media is proportional to wavelength, the longer the wavelength the deeper the penetration. Therefore, the lower frequency content of UWB transmissions would have greater penetration abilities to detect deeply buried bunkers. Similarly, radar detection or communication through walls and floors requires lower frequencies for optimal operation. Measurements show that attenuation through a concrete wall is roughly $10f_o\ dB/m$, where f_o is the operating frequency in GHz [7]. Thus to penetrate, the lowest possible frequen-

cies are needed, but high resolution is required to resolve multipath reflections or image objects. Therefore, the optimum device to communicate or image through a concrete wall is one that operates at the lowest possible frequency, yet provides the best resolution at those low frequencies. This is one of the principal characteristics of the UWB waveform-ultrawide relative bandwidth [3].

1.3.3 Target Imaging and Discrimination. Since time and frequency resolution are inversely proportional, wider bandwidth produces finer time resolution. UWB waveforms provide optimal resolution at the lowest possible frequency and when combined with the other waveform characteristics, mitigate multipath by both resolving it and reducing it. Once resolved, RAKE processing is applied to UWB communication signals to mitigate multipath by phase correction and coherent addition to form the final received signal. This discrimination methodology gives UWB systems spatial diversity that can add reliability and reduce the power required to support a desired range and data rate [3].

1.3.4 Secure Communication. UWB signals can also provide secure communications. This is an important benefit that can be exploited for covert operations or preventing theft of service. As stated earlier, UWB devices produce LPI/LPD signals. Visually a signal's detectability comes from how "spiked" it appears to the instrument used to interrogate it. That is, signals are hard to detect if they have low peak-to-average ratios in the domain of the interrogating instrument. For instance, UWB signals that are properly modulated appear smooth in the frequency domain and are therefore hard to detect on a spectrum analyzer [3]. From an implementation standpoint, UWB system are favored as well since they can be implemented without a modulating carrier thereby simplifying the transmitter and receiver design.

One of the most recent applications of UWB communications technology is to the development of highly mobile, multi-node, ad hoc wireless communications networks for the DoD. One tested system provided a secure, low probability of inter-

cept and detection, UWB ad hoc wireless network capability to support encrypted voice/data (up to 128 kb/s) and high-speed video (1.544 Mb/s) T1 transmissions [8].

1.3.5 High Capacity Networks. The UWB bandwidth generates substantial interest in communications and networking arenas since it has been shown that UWB can transfer data at ranges up to 30 feet and at throughput ranging from 100 to 500Mbps [9]. Industry experts expect to field intra-room wireless systems within the next two years.

With the high processing gain of a UWB system comes an implied large code space. A large code space allows for many low cross correlation codes as discussed in Section 2.3. The large number of good codes enables high connectivity, both in terms of simultaneous users and the pool of unique addresses. UWB systems can have orders of magnitude more simultaneous users in a cell, with the same data rate and multi-user interference level, when compared to a conventional spread spectrum system [3]. Simply stated, a UWB system is capable of supporting more users in a faster network.

1.4 Problem Statement and Scope

The increasing demand for portable, high data rate communications has focused much attention on wireless technology. Ultra Wideband (UWB) waveforms have the ability to deliver megabits of information while maintaining low average power consumption. In accordance with the April 2002 FCC First Report and Order, UWB systems are now allowed to operate in the unlicensed spectrum of 3.1 to 10.6 GHz [10]. The order has motivated renewed interest in the forty-year-old concept of impulse signaling as applied to the three categories of approved UWB devices: 1) imaging systems including Ground Penetrating Radars (GPRs), through-wall, surveillance, and medical imaging devices, 2) vehicular radar systems, and 3) communications and measurement systems.

Gaussian monocycles are a class of UWB waveforms offering large bandwidths and enabling multiple access (MA) capability through "spreading" techniques. Although both Time Hopping (TH) and Direct Sequence (DS) MA modulation techniques are available, only time hopping is considered in this research to provide a UWB MA capability.

This work extends previous UWB multiple access (MA) performance characterization by combining Gold coded, Time Hopped Pulse Position Modulation (TH-PPM) with 4-Ary biorthogonal communication signaling, referred to here as TH-BPPM MA signaling. It also evaluates communication performance using a "fast hopping" modulation technique using 1, 2, and 10 hops per symbol. *Matlab*® is used to simulate probability of bit error (P_b^H) under multiple access interference (MAI) and multipath interference (MPI) conditions for both synchronous and asynchronous networks containing up to 15 transmitters.

1.5 Methodology

Matlab® was used to simulated end-to-end UWB network communication performance. The network consisted of 1-15 transmitters, 1-15 direct signals and 40 multipath replications per transmitter, and a correlation receiver for the signal of interest. UWB symbol generation, transmission, detection and estimation were entirely software driven to permit control and variation of key parameters. The model is validated using theoretical models for antipodal and orthogonal signaling and subsequently extended to include simulated network performance with multipath, multiple access, and "spread spectrum" fast hopping schemes.

1.6 Equipment

Matlab® Versions 6.1.0.450 (Release 12.1) and 6.5.0.180913*a* (Release 13) were used for algorithm development and execution. The *Matlab*® programs resided on multiple personal computers; the typical configuration was a Dell Personal Computer

with an Intel® Pentium® 4 processor operating at 2.53 Gigahertz, 1.047 Gigabytes of random access memory, and Microsoft Windows 2000, (Service Pack 4) operating system.

1.7 Thesis Organization

This document is organized into five chapters. Chapter 1 introduces (UWB) communication concepts and lays out the structure of the thesis document. Chapter 2 provides UWB background information based on relevant literature and previously research efforts. Chapter 3 details the research methodology. Chapter 4 presents the model validation and simulated network performance results. Chapter 5 provides conclusions and potential research topics related to this thesis. The appendices contain the algorithm code and additional simulation results.

II. Background

2.1 History

Several terms have been used over time to reference UWB waveforms. Nonsinusoidal, base-band [11], impulse radio, and carrier free signals are just a few of the terms used in literature to describe UWB signals. The term "UWB" was not adopted until about 1989. Dr. Gerald F. Ross first demonstrated the feasibility of utilizing UWB waveforms for radar and communications applications in the late 1960s and early 1970s [11]. The key to actual realization of a physical system came with the development of the avalanche transistor and tunnel diode. Initially, a nanosecond rise time pulse could be generated but there wasn't any test equipment with a fast enough response to actually capture the signal. This changed as sampling oscilloscopes entered the market to further aid system development. Throughout the 1970s, UWB research focused on enhanced resolution for radar systems which demanded wider bandwidth. Research was not limited to American scientists; Russian researchers Astanin, Kosylev, Fedotov, and Immoreev published detailed analysis of UWB in a multitude of applications. One of the principal American figures over the last decade has been Lieutenant Colonel (retired) James D. Taylor. Taylor was chief of Advanced Technology Planning at the Air Force Electronic Systems Division, when he organized the first American UWB radar symposium, promoted early research work on defense applications, and authored "Introduction to Ultra-wideband Radar Systems" (1995) [12] for CRC Press.

During the last decade, the military has begun to support initiatives for developing commercial applications. These commercial applications, and the evolution of increasingly faster digital circuits, have led to the development of inexpensive hardware. Additionally, the ability to produce low cost units and unlicensed use have recently boosted interest in UWB.

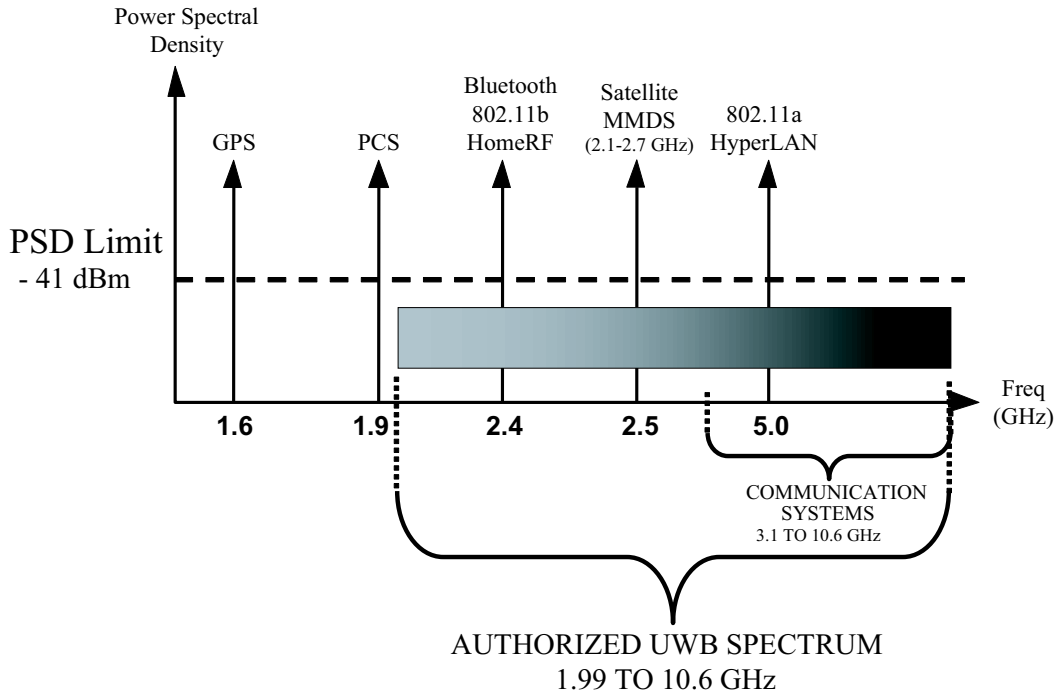

Figure 2.1: Ultrawideband frequency spectrum range as compared to Global Positioning System (GPS), Personal Communication System (PCS) i.e., Palm Pilot, and common network protocol frequency spectrums

The FCC has been extremely cautious in allowing the use of UWB systems due to possible signal interference issues. Figure 2.1 shows the broad spectral region available to UWB transmissions and highlights the overlap with operational systems and standards.

The multitude of potentially affected systems has slowed Government approval to ensure that UWB devices do not negatively interfere with currently fielded electronic devices. In April 2002 the FCC published the First Report and Order [1] guiding UWB development and subsequent system approval. The order established different technical standards and operating restrictions for four types of UWB devices based on their potential to cause interference. These UWB devices were categorized as:

Table 2.1: FCC EIRP Emission Limits (dBm)

	Imaging Systems					
Frequency (MHz)	Low Freq	Medium Freq	High Freq	Indoor	Vehicle Radar	Hand Held
Below 960	-	15.209 Limits	15.209 Limits	-	-	-
960-1610	-65.3	-53.3	-65.3	-75.3	-75.3	-75.3
1610-1690	-53.3	-51.3	-53.3	-53.3	-61.3	-63.3
1990-3100	-51.3	-41.3	-51.3	-51.3	-61.3	-61.3
3100-10600	-51.3	-41.3	-41.3	-41.3	-61.3	-41.3
10600-22000	-51.3	-51.3	-51.3	-51.3	-61.3	-61.3
22000-29000	-51.3	-51.3	-51.3	-51.3	-41.3	-61.3
29000-31000	-51.3	-51.3	-51.3	-51.3	-51.3	-61.3
Above 310000	-51.3	-51.3	-51.3	-51.3	-61.3	-61.3

1. Imaging Systems (Ground Penetrating Radars, through-wall, surveillance, and medical imaging devices)
2. Vehicular Radar Systems
3. Indoor UWB Systems
4. Hand Held Devices

The FCC adopted unwanted emission limits for UWB devices that are significantly more stringent than those imposed on other devices. The First Report and Order also contained emissions masks limiting the frequency band within which certain UWB products would be permitted to operate. The frequency band of operation is based on the 10 dB bandwidth of the UWB emission as shown in Fig. 2.2. Table 2.1 outlines the Effective Isotropic Radiated Power (EIRP) by frequency band for different systems. Figure 2.3 graphically illustrates the mask imposed on indoor and outdoor (hand held) UWB systems. The combination of technical standards and operational restrictions were established to promote development and to ensure that UWB devices could coexist with authorized radio services without the risk of harmful interference while gaining experience with this new technology [1].

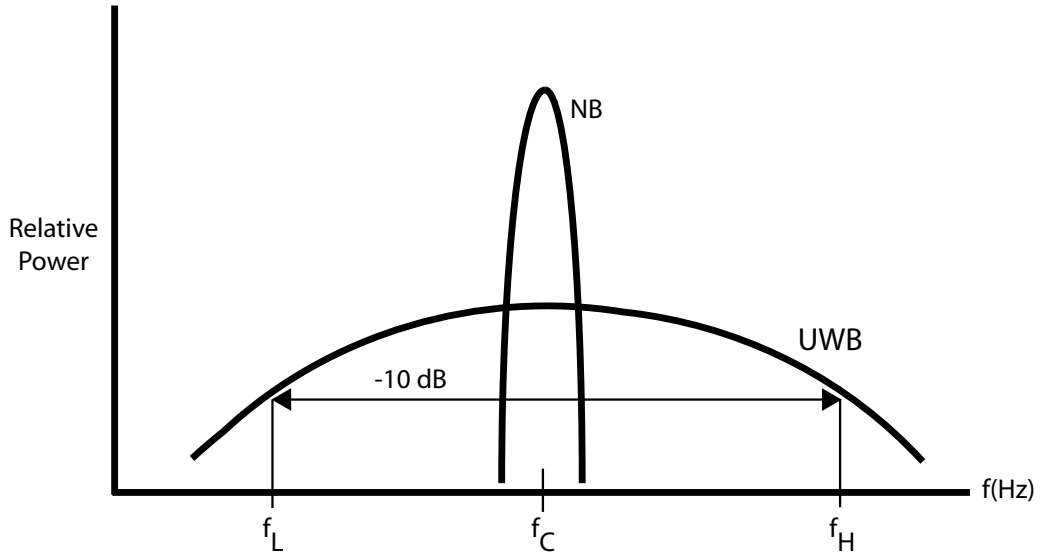

Figure 2.2: UWB Fractional Bandwidth

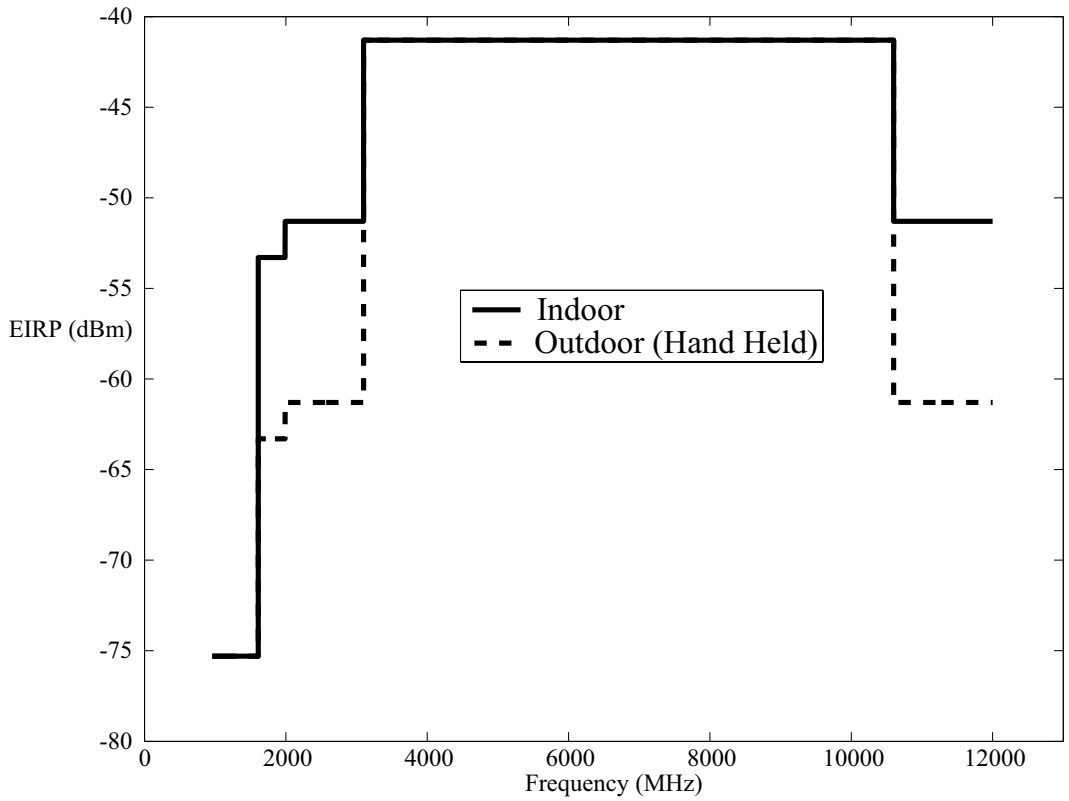

Figure 2.3: Indoor and Outdoor (Hand Held) UWB Frequency Mask Imposed by FCC

2.2 UWB Waveform Modeling and Phenomenology

2.2.1 UWB Signals Defined. Analysis of UWB signals begins with a detailed characterization of the waveform and its spectrum. Signals are categorized into three main classes, narrowband (NB), wideband (WB), and ultrawideband (UWB) based on fractional bandwidths of less than 1.0, 1.0 to 25.0, and greater than 25%, respectively. Fractional bandwidth (B_f) is defined as [10]

$$B_f = 2\left(\frac{f_H - f_L}{f_H + f_L}\right) \tag{2.1}$$

where f_H and f_L are the upper and lower frequency emission points which are 10 dB below the peak responses as indicated in Fig. 2.2. The center frequency (f_C) of the transmission is defined as the average of the upper and lower 10 dB emission points, i.e., $f_C = (f_H + f_L)/2$. The low power and gigahertz (GHz) bandwidth are the characteristics currently being exploited by radar and communications engineers. The UWB signal effectively spreads energy over a large spectral region and has a low power spectral density (watts/hertz); such waveforms are commonly used for low probability of intercept or detection applications. Thus, UWB signaling is highly useful for military applications requiring covert communication in hostile environments.

2.2.2 The Gaussian Monopulse. Figure 2.4 depicts the time domain and frequency domain representations of a UWB Gaussian monopulse, a commonly modeled output of a UWB transmitter. In many practical applications, an individual data bit is comprised of multiple Gaussian monopulses. The spectrum generated by a uniformly spaced pulse train of Gaussian monopulses can wreak havoc in a multiple access environment. The pulse train creates multiple spectral lines that could lead to massive destructive collisions whenever several pulses from two signals are received simultaneously. The line spectra can be "smeared" by randomly shifting the pulses in time through dithering or time hopping. Figure 2.5 shows the effects of uniform

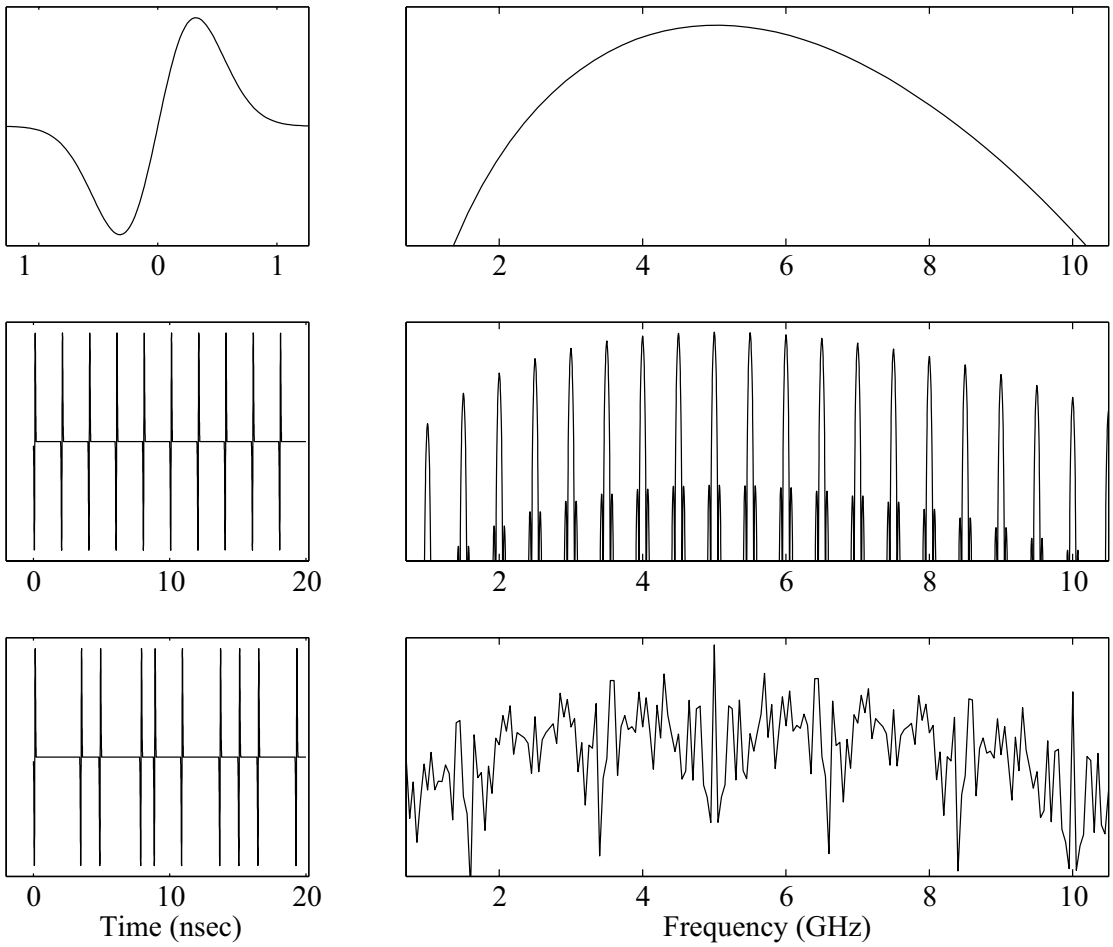

Figure 2.4: Temporal (left-hand plots) and spectral (right-hand plots) characteristics of Gaussian monopulse (top), uniformly spaced pulse train (middle), and fast time hopped pulse train (bottom)

spacing and fast time hopping on the spectral envelope. The changes in smoothness from the monopulse to the uniform pulse train, and the smoothing effects of the fast time hopped pulse train are apparent. The shape of the envelopes remains relatively constant though the instantaneous values differ significantly, especially in the case of the uniform pulses.

Figure 2.4 graphically shows temporal and spectral characteristics of a single monopulse, a uniformly spaced pulse train of Gaussian monopulses, and a fast time hopped pulse train of Gaussian monopulses. The uniform pulse train's narrow line

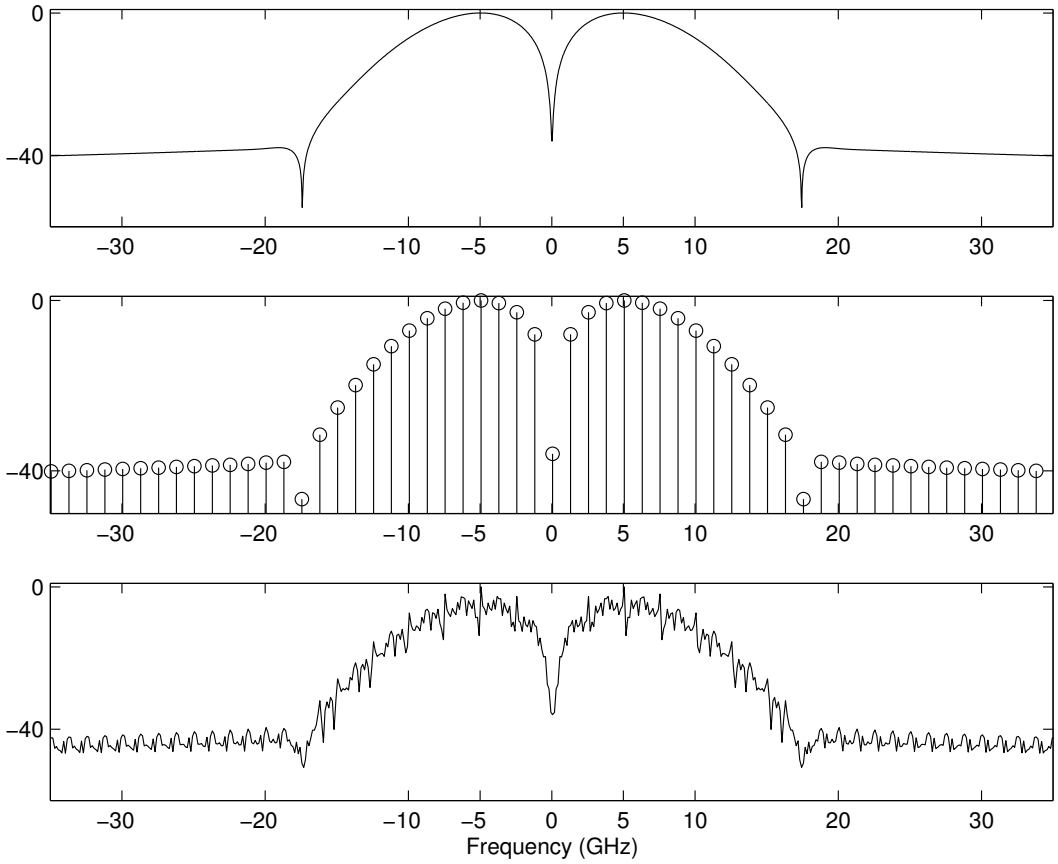

Figure 2.5: Frequency envelopes of Gaussian monopulse (top), uniformly spaced pulse train (middle), and fast time hopped pulse train (bottom)

spectra is evident in in the middle frequency plot. A single jammer operating within a narrow range could negatively impact system performance. The smoothing effects of only slightly time hopping 10 pulses is shown in the bottom right-hand plot of Fig. 2.4. In a fast time hopped pulse train environment, any potential jammer would have to cover a much larger bandwidth making it impractical to implement.

2.2.3 Transmitted Waveform. The second derivative of a Gaussian monopulse is modeled as the received UWB pulse to maintain consistency with [2]. Accounting for wave shaping effects of the transmit and receive antennas, the second

derivative waveform is represented in the time domain by

$$w(t) = \left[1 - 4\pi \left(\frac{t}{\tau_m}\right)^2\right] \exp\left[-2\pi \left(\frac{t}{\tau_m}\right)^2\right] \tag{2.2}$$

where the impulse width parameter τ_m is approximately equal to 0.4 times the pulse width T_w. Basic UWB Pulse Position Modulation (PPM) can be achieved with

$$s_i(t) = w\left[t - (-1)^{a_i} \cdot \Delta\right] \tag{2.3}$$

where i is the symbol number, a_i is the binary input data qualing 1 or 0, and Δ is the relative PPM offset. The resulting binary PPM waveforms of (2.3) with $T_w = 0.2\ nsec$ (5 GHz operation) are shown in Fig. 2.6.

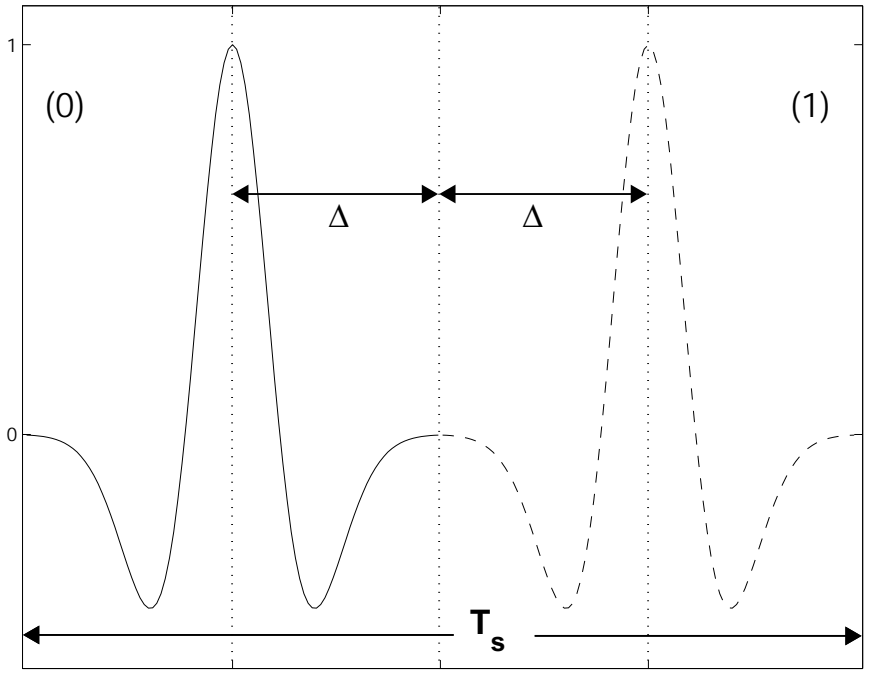

Figure 2.6: Binary Pulse Position Modulation Offset

2.2.4 Symbol Generation. Biorthogonal signals, as defined in [13], are two sets of orthogonal signals such that each symbol in one set has an antipodal

symbol in the other set. Biorthogonal PPM (BPPM) is achieved by combining binary PPM with antipodal signaling. The resultant communication symbols using the fundamental UWB waveform of (2.2) are shown in Fig. 2.7 and can be analytically represented by [14, 15]

$$s_i(t) = (-1)^{a_{2i}} \cdot w\left[t - (-1)^{[a_{2i} \oplus\ a_{2i-1}]} \cdot \Delta\right] \tag{2.4}$$

for $t_i \leq t \leq t_i + T_s$ where i is the symbol number, a_{2i} and a_{2i-1} are the binary input data equaling 1 or 0, $\oplus$ represents modulo-2 addition, T_s is the symbol duration, and Δ is the relative PPM offset.

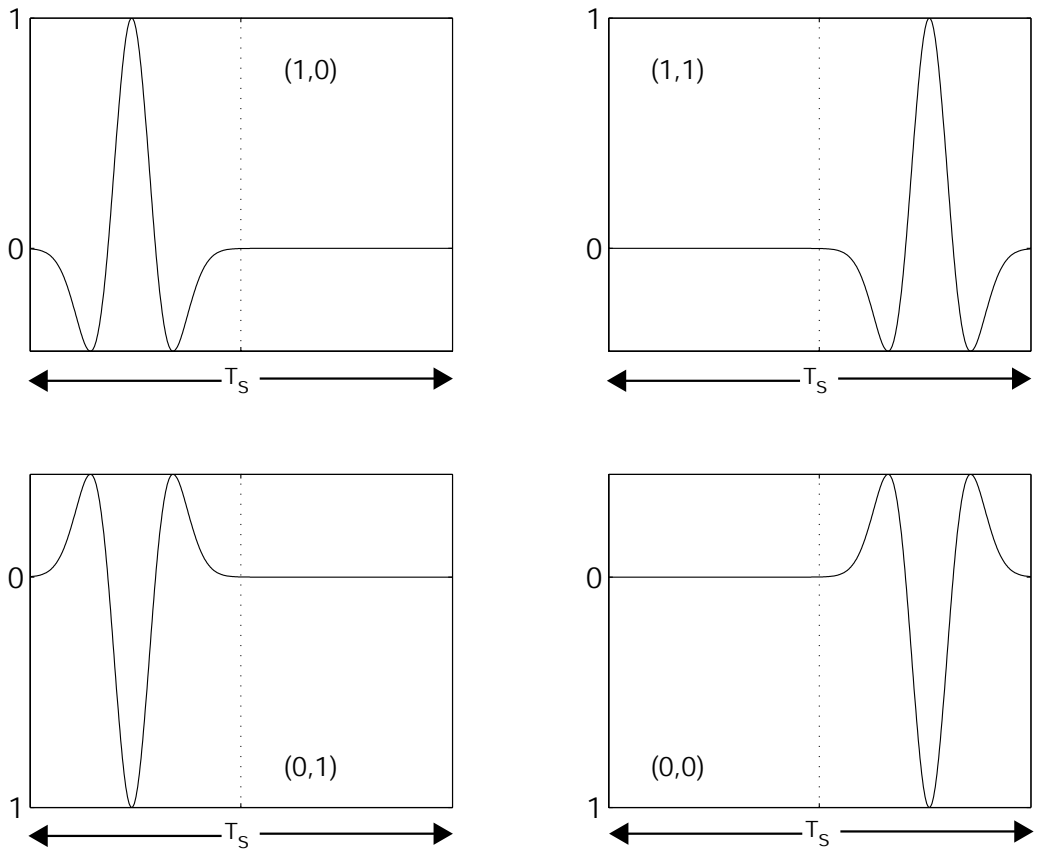

Figure 2.7: 4-ary Biorthogonal UWB Waveforms Generated from (2.2) and (2.4) Using Bit Patterns of (a_{2i-1}, a_{2i}) as Indicated [14]

2.2.5 Multiple Access via Time Hopping. Time hopping UWB modulated signals in accordance with preassigned coding, such as that presented in Section 2.3, is one common technique for providing multiple access (MA) capability [16]. In the TH-BPPM technique, the signal information contained in both relative pulse position and amplitude characteristics is preserved upon implementing MA capability. This information can be reliably recovered using temporal "spreading", i.e., repeating communication symbols across time, in a manner paralleling the fast frequency hopping technique commonly used for spectral spreading. The 4-ary biorthogonal modulated signals described by (2.4) are used in conjunction with preassigned, uniquely coded time hopping sequences to implement MA capability. The analytic representation for the biorthogonal TH-BPPM MA technique follows directly from the orthogonal TH-PPM MA technique commonly used in research [16,17], with the k^{th} user's signal is given by

$$s^{(k)}(t) = \sqrt{P_k} \times \sum_{i=1}^{\infty} \sum_{j=(i-1)\cdot N_H}^{i\cdot N_H - 1} s_i \left[t - jT_o - c_j^{(k)} T_c \right] \tag{2.5}$$

where P_k is the average power, N_H is the number of hops per communication symbol, T_c is the chip interval (the time allotted for one M-ary symbol), T_o is the symbol repeat interval, $\{c_j\}$ is the chip offset sequence with period N_c, with $\{c_j\}$ equal to $\{c_0, c_1, ..., c_{N_c-1}\}$, and $c_j \in \{1, 2, 3, ..., N_c\}$.

Each communication symbol of (2.4) repeats N_H times and occurs once within each T_o at a position dictated by c_j as shown in Fig. 2.8. As indicated in (2.5), sequential c_j values are used for the N_H repetitions of the original symbols, i.e., c_j values are **not** constant over N_H repetitions; every symbol is offset by a sequential c_j.

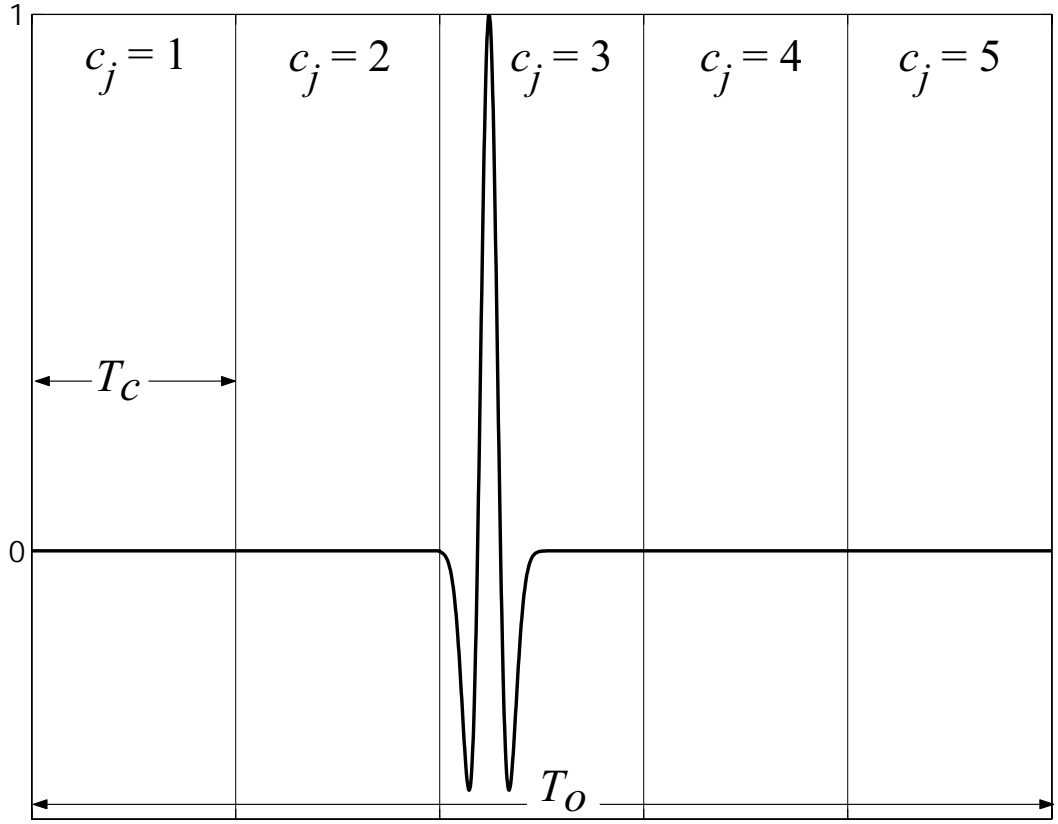

Figure 2.8: Example of TH-BPPM for $N_c = 5$ Chips per T_o, Symbol (1,0), and $c_j = 3$

2.3 Multiple Access Code Generation and Selection

Multiple access capability can be achieved for all $N_H \geq 1$ where a processing gain of N_H is realized. In this case, signal discrimination for the k^{th} user is obtained by applying chip offsets $c_j^{(k)}$ derived from pseudorandom sequences. For consistency with previous work [17], 31 length Gold codes are used to generate chip offset sequences. Gold coding is a reasonable choice given the large number of available codes and the well-defined periodic cross-correlation (R_{XY}) characteristics [18]. The coding provides the added benefit of time hopping the transmitted waveforms thereby mitigating the line spectra issues discussed in Section 2.2.2.

Carefully chosen pairs of maximal length sequences (m-sequences) can be used to generate a family of Gold code sequences. One key characteristic of Gold codes

is the cross correlation of any two codes in the family produces is three valued, which allows the receiver to distinguish the signal of interest in a multiple access environment. The three Gold code cross-correlation values are easily calculated using [19]

$$R_{XY} \in \left\{1, \frac{-1}{N}, \frac{-\beta(n)}{N}, \frac{\beta(n)-2}{N}\right\} \tag{2.6}$$

where $\beta(n) = 1 + 2^{\lfloor \frac{n+2}{2} \rfloor}$, N is equal to the code length, $n = log_2(N+1)$, and $\lfloor a \rfloor$ denotes the greatest integer less than a. Typical normalized Gold code autocorrelation and cross correlation responses are illustrated in Fig. 2.9.

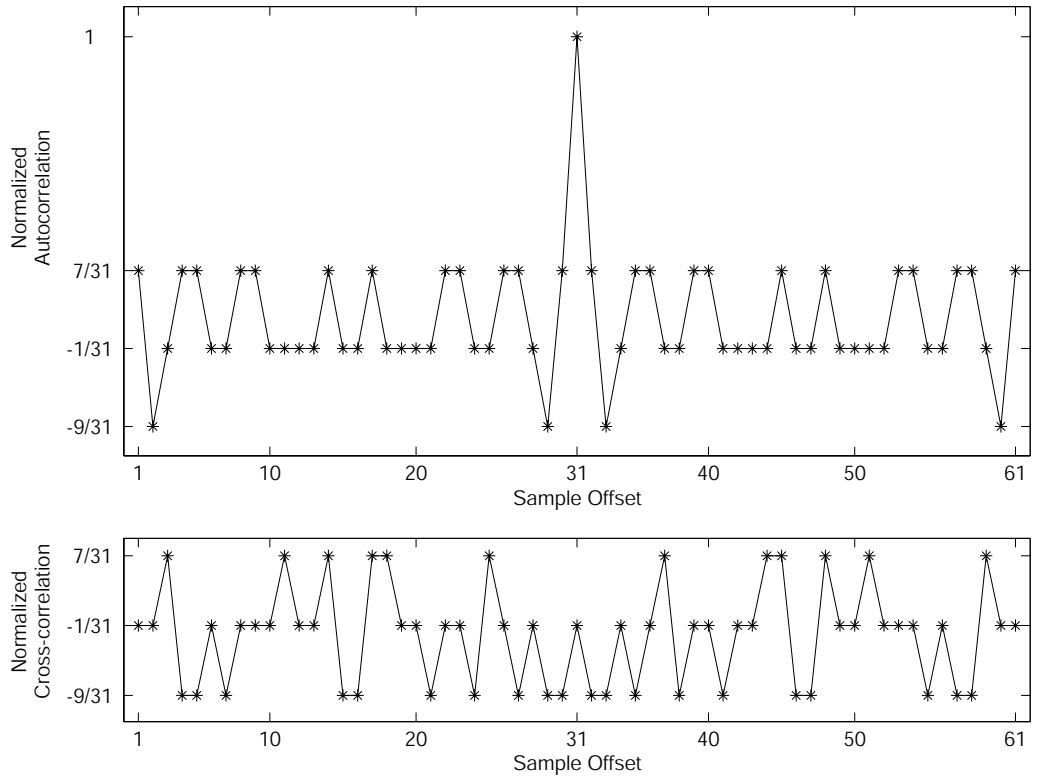

Figure 2.9: Typical Normalized autocorrelation (top) and cross correlation (bottom) responses for a Gold code (31-length Illustrated)

Figure 2.10 demonstrates a mechanism for deriving chip offset sequences from Gold code sequences by mapping (binary-to-decimal conversion) Gold code elements to integer values using an r-element ($r = 5$) wide sliding window and single code

element shifts. The choice of r is significant because 1) it determines the maximum number of transmitters on any given network based on the number of unique codes available and 2) the number of offsets 2^r multiplied by the chip interval (T_c) sets the symbol repetition interval (T_o), all of which relate to data rate and network throughput. The r should be maximized such that $2^r - 1$ equals the respective code length. Using a large r maximizes the resulting code space and thereby minimizes possible collisions with multiple transmitters. For l-length Gold codes, the conversion process provides unique l-length user TH code set where $c_j \in [0, 1, ..., 2^r - 1]$ with periodicity $N_c = 2^r$ such that $c_j = c_{j+nN_c}$ for all n.

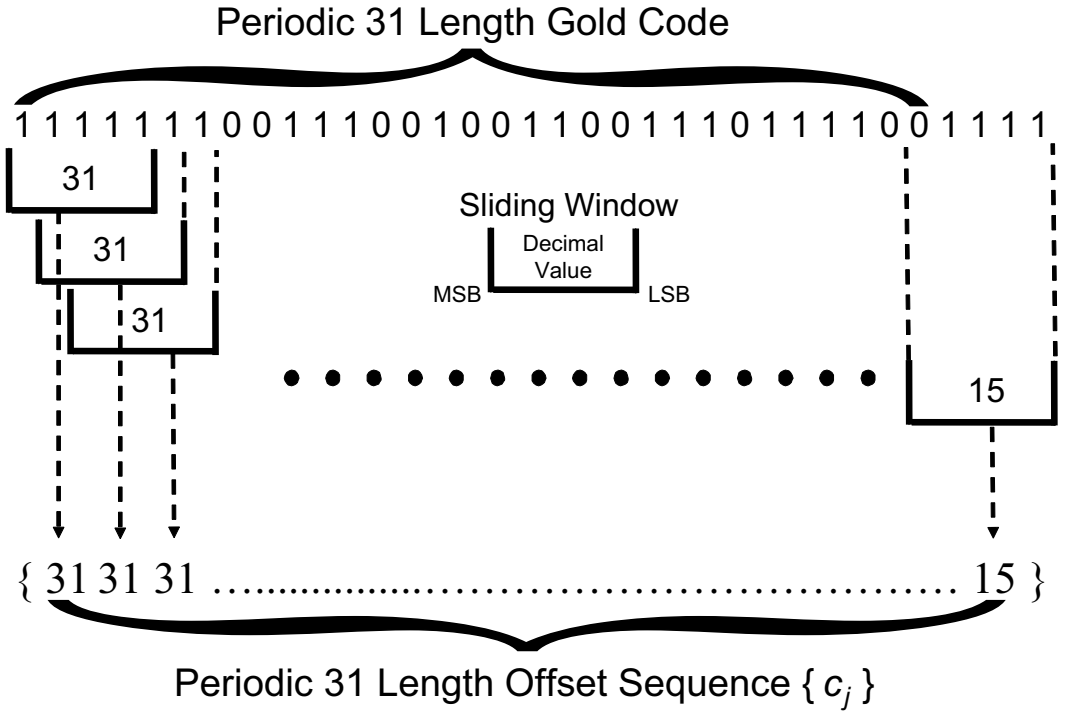

Figure 2.10: Code Gold 31 Binary to Decimal Conversion

2.4 Interference Factors

A communication system's bit error performance is directly related to E_b/N_o into the demodulator, where E_b is the energy per bit and $N_o/2$ is the 2-sided noise spectral density. The E_b/N_o is in turn directly related to the received signal's signal-

to-noise ratio (SNR) by

$$\frac{E_b}{N_o} = \frac{S\,T_s/k}{N\,2/W} = \left(\frac{S}{N}\right)\,\frac{T_s}{k\,\Delta t\,2} \tag{2.7}$$

where T_s is the symbol duration, $W = 1/\Delta t$ is the signal bandwidth, Δt is the sample spacing, and k is the number of bits per symbol ($k = 2$ for 4-ary modulation). Though E_b/N_o provides an easy means for determining expected performance, the ratio of bit energy to noise power spectral density is not as easily visualized, or measured, as SNR. Given fixed transmitter strength, S can only decrease while propagating while total noise power N can be affected by numerous sources. In an extreme environment, transmitted signals are subject to a multitude of interferers including multiple transmitters (MA), multiple signal reflections (multipath), noise added in the transmission channel, and even intentional jammers. A simple model of received SNR (SNR_r) can be viewed as

$$\begin{aligned} SNR_r &= \frac{Average\ Received\ Signal\ Power\ (S_r)}{Average\ Received\ Noise\ Power\ (N_r)} \\ &\approx \frac{S_r}{MAI + MPI + AWGN + J} \end{aligned} \tag{2.8}$$

where MAI is the interference from multiple transmitters, MPI is multipath interference, $AWGN$ is additive white Gaussian noise, and J is additional jammer interfering power.

Although UWB communication systems are a relatively new field of study, the body of work addressing channel modeling which takes into account each of the above effects is growing. In-depth studies on channel effects have been reported by [20–22]. A UWB receiver's ability to resolve a large number of multipath sources has garnered interest. Numerous channel models have be examined for validating against fielded hardware. Rayleigh fading is commonly applied in communication path loss models but laboratory results of fielded systems show that log-normal may

be more appropriate for UWB systems [23]. Additionally, [21] proposes a Markov $(\Delta - K)$ model to characterize arrival time of multipath signals which indicated strong correlation between analytic and experimental results. A detailed examination of multipath interference effects for indoor wireless channels can be found in [24]. In [25], researchers conducted a signal propagation experiment in a general office environment to investigate multipath. They concluded rather succinctly that UWB signaling does not suffer multipath fading.

III. Methodology

3.1 Problem Definition

The objective of this research is to develop an analytical model which accurately characterizes the expected communication performance of a UWB TH-BPPM transmission system. Fast time hopping is implemented to improve performance in a multiple access/multiuser interference environment (MAI). Additional interference in the form of Additive White Gaussian Noise (AWGN), and multipath (MPI), delayed versions of the original signals, for synchronous and asynchronous transmission modes complete the performance analysis. The model's performance in a single user, zero multipath environment is validated against results reported in [2] and analytic equations for equivalent Gray-coded QPSK modulation.

A communication system's bit error rate (a key performance metric) degrades in the presence of other interfering signals. Bit error rate is merely the ratio of bits received and estimated in error divided by the total number of transmitted bits. Each interference factor (AWGN, MAI, and MPI) are varied to determine the individual impact on system performance. Combined interference effects, culminating in a hostile environment comprised of all forms of interference, are then considered.

Signal-to-Noise ratio (SNR) is a common term to indicate the "strength" of a received signal. However, in digital communications, the available E_b/N_o into a demodulator determines the receiver's ability to properly estimate the received signal. The relationship between SNR and E_b/N_o was shown in Section 2.4. Acceptable bit error performance is one design factor for the communication system design engineer. The results presented herein will allow direct comparison with previously published results of other UWB modulation schemes.

3.2 System Boundaries

Characterization of the UWB TH-BPPM system begins with the development of an analytical model using a Matlab® implementation scheme as outlined in Fig. 3.1. The UWB transmitter described by [2] is used as a baseline and modified for the 4-ary signal constellation and fast time hopping environment.

3.2.1 System Under Test. The system under test (SUT) consists of two active components, the UWB transmitter and UWB receiver, and a passive component, the transmission medium – free space. From a macro perspective, a pulse generator within the transmitter creates the desired UWB Gaussian waveform. The waveform passes into the modulator where, depending on the current k data bits at the demodulator, it is converted to one of M symbols using Pulse Position Modulation (PPM) and antipodal signaling. The waveform then enters the multiple access encoder which applies the Time Hopping (TH) code presented in Section 2.3 and Section 3.6.6.

To simulate real-world channel effects, MAI and MPI are added following MA signal generation [2]. AWGN is combined to establish a SNR_r based upon the user defined E_b/N_o. As indicated above, multiple independent waveforms are generated and unique user codes are applied to provide MAI. MPI is inserted by randomly delaying superposed replicas copies of the desired signal, plus any MAI, waveform(s). Different realizations of AWGN are added to each of the waveforms and superposed to create the composite received waveform. Separate iterations are performed to assess performance in synchronous and asynchronous networks.

All despreading and demodulation is performed within the detection and estimation stage described in Section 3.7. For this research, the received signal of interest is assumed to be properly synchronized. All user codes and number of hops per symbol (N_H) are known a priori which allows the correlator to integrate over

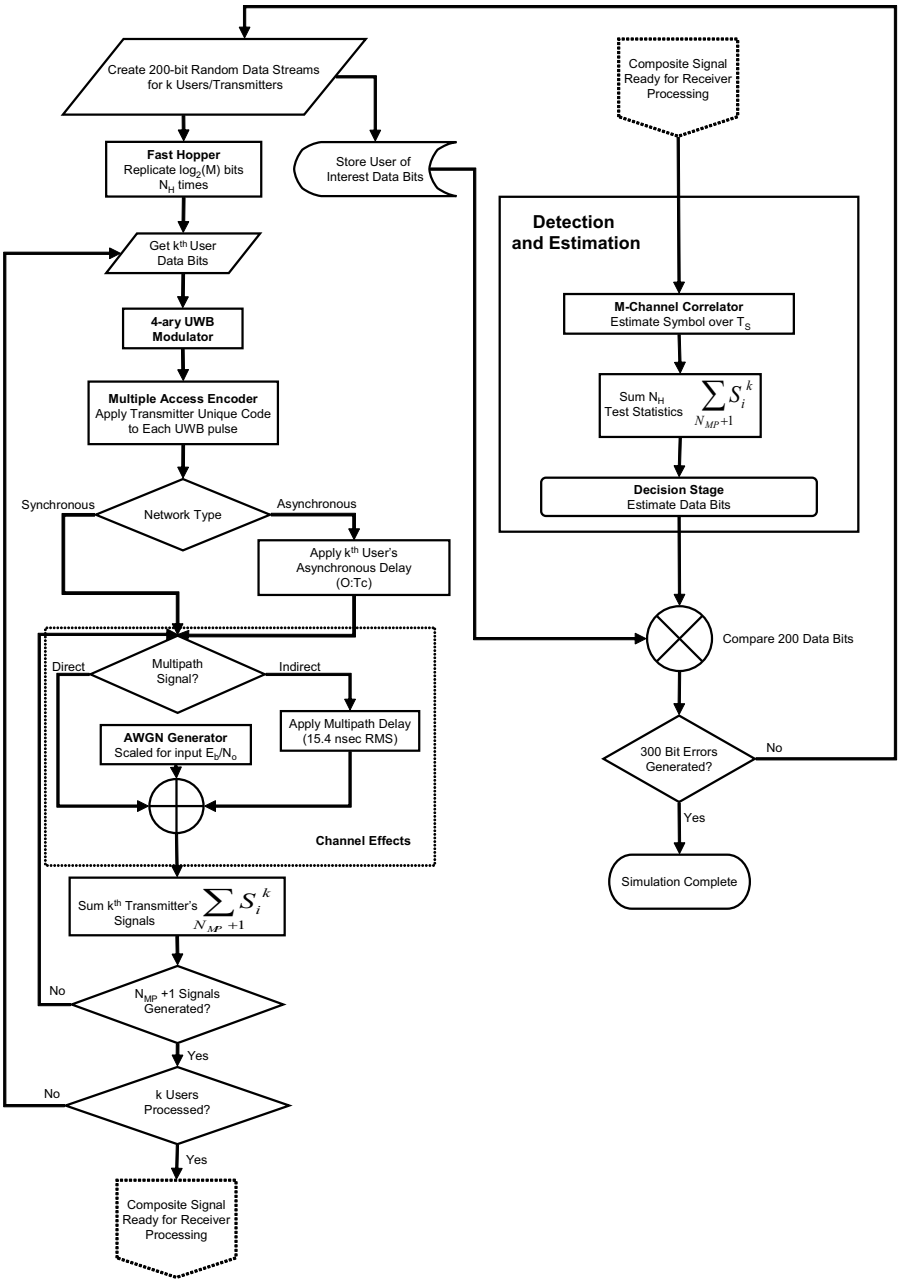

Figure 3.1: Simulation Flowchart

one symbol interval (T_S). The estimated data bits are compared bit-by-bit to the original input at the transmitter modulator to derive the bit error rate.

3.2.2 System Limitations. As with any simulation, real world effects cannot be fully implemented given the processing constraints. The following limitations were implemented to permit comparison with previously published data:

Channel Fading: No channel fading models, such as the Rayleigh, log-normal, or Markov-K were applied the generated waveforms. All multipath and direct signals contained equivalent signal strength contributions from the UWB pulses.

RAKE Receiver: It has been shown [20] that improved performance in a UWB environment can be achieved using a RAKE receiver. RAKE was **not** used in this study. The receiver is a four channel correlator/accumulator combination.

Pulse overlap: Symbol duration T_S and PPM offset Δ were made sufficiently large enough to provide zero overlap of pulses within the set of four communication symbols. A relative PPM offset of $\Delta = T_s/4 = T_w/2 = 0.1\ ns$ was used (cf., Fig. 2.6) resulting in the 4-ary symbols (cf., Fig. 2.7).

Multipath: Multipath can be modeled multiple ways, i.e., a different delay could be applied to each pulse, to each message (comprised of N_H pulses per symbol), or to each multipath link. The approach herein was to vary the multipath value message-to-message. Some studies have reported root mean square (RMS) delays of 25 to 50 nanoseconds. For comparison with [2], the value is set at 15.4 nanoseconds as reported in [24].

3.3 System Services

Effective communication is defined by the message received equalling the message transmitted. Put in simple terms, the ones and zeros (bits) out of a receiver should equal the ones and zeros into the transmission system and be in the same order. Unfortunately, degradation occurs in a wireless transmission when the original bits are converted to an analog form for propagation. The transmission through free space imparts losses and interference corrupts the electromagnetic waveform.

Thus a noisy, weaker signal is received by a less than perfect antenna for reconstruction by the receiver into a digital waveform. The ultimate service provided is data/message transfer and the "goodness" of the system is characterized by how often it reconstructs the signal correctly.

3.4 Performance Metrics

Data analysis consists of characterizing communication performance of the UWB TH-BPPM signal in various multiple access and multipath environments. The true figure of merit for any communication system is the probability of bit error (P_b) in a given transmission. The confidence and accuracy of the P_b results can be quantified using network performance equations from [26] where the Confidence Interval ($C.I.$) is given by

$$C.I. = P_b \mp z_{(1-\alpha/2)} \cdot \sqrt{\frac{P_b \cdot (1 - P_b)}{n}} \; for \; n \cdot P_b \geq 10 \tag{3.1}$$

where P_b is equal to the number of bit errors divided by the total number of bits generated in the simulation (n), α is the significance level, and $z_{(1-\alpha/2)}$ is the $(1 - \alpha/2)$-quantile of a unit normal variant. The accuracy (r) is merely one-half the variance of the C.I. values and is given by

$$r = z_{(1-\alpha/2)} \cdot \sqrt{\frac{P_b \cdot (1 - P_b)}{n}}). \tag{3.2}$$

Simulation time can be significantly reduced by limiting the number of errors required to meet C.I. and accuracy requirements. Computer processor speeds allowed pilot simulations to accrue 300 errors before terminating. Subsequent simulations used the same 300 error minimum which assured the $n \cdot P_b \geq 10$ requirement of (3.1) was met. With 300 errors as a constant, the theoretical value of n varied as a function of required P_b, i.e., a $10^{-6} = P_b = 300/n \Rightarrow n = 300 \cdot 10^6 \; bits$. Therefore,

given the following parameters, the bounded C.I. accuracy can be calculated as

$$
\begin{aligned}
P_b &= 10^{-6} \\
\textit{Bit errors} &= 300 \\
n &= 300 \cdot 10^6 \\
C.I. &= 95\% \\
\alpha &= 0.05 \\
z_{(1-\frac{\alpha}{2})} &= 1.96 \\
r &= 1.96 \cdot \sqrt{\frac{10^{-6} \cdot (1 - 10^{-6})}{300 \cdot 10^6}} \approx 1.13 \times 10^{-7} \\
C.I. &= P_b \mp r \\
C.I. &\approx 10^{-6} \mp 1.13 \times 10^{-7}.
\end{aligned}
$$

The r value only improves as P_b decreases; for P_b of 10^{-2} through 10^{-6}, the accuracy improves from approximately 1.13×10^{-3} to 1.13×10^{-7}. Though the accuracy may improve in terms of raw numbers, the percent error P_b/r remains nearly constant at approximately 10% for all results presented in Chapter 4.

3.5 Parameters

A communication system model is comprised of a multitude of possible parameters defining the particular system. Multiple access using a fast time hopping algorithm in a multipath environment provides the basis of this work. The basic waveform structure must remain constant to accurately compare performance levels. Table 3.1 identifies the principal parameters addressed in this research. Those with fixed values are associated with the basic waveform structure. The waveform structure is similar to that reported in [2]. In generating the waveform, pulse duration T and repetition interval T_o control the frequency range over which the system operates. For example, a pulse gated on every $T_w = 0.2$ *nsec* is spectrally centered

at 5.0 GHz. Pulse duration must be closely controlled since the center frequency is inversely proportional. A small error in pulse width can move system operation outside the bandwidth of receiver filters. Chip time T_c and the length of the Chip Offset Sequence c_j control the Symbol Repeat Interval T_o. Therefore, T_o is set to $N_c \times T_c$.

Table 3.1: Principal System Parameters

Parameter	Symbol	Value
Pulse duration	T_w	$0.2 \times 10^{-9} s$
Pulse width parameter	τ_m	$0.4 \times T = 0.8 \times 10^{-10} s$
Pulse Repetition Interval (PRI)	T_o	$T_c \times 2^r = 12.8 \times 10^{-9} s$
A/D sampling resolution	dt	$8.0 \times 10^{-12} s$
Chip duration	T_c	$2 \times T = 0.4 \times 10^{-9} s$
PPM Offset	Δ	$T_w/2 = 0.1 \times 10^{-9} s$
User Code	c_j	Defined in Section 3.6.6
Sliding window width	r	5
Number of multipath	N_{MP}	{0, 5, 10, 20, 40}
Number of transmitters	N_T	{1, 2, 3, ..., 15}
Number of hops per symbol	N_H	{1, 2, 10}
Signal energy	E_b/N_o	Based on N_H and required BER
Asynchronous Offset	$Async$	Random $[0 : T_c]$

Variations in the parameters of Table 3.1 dictate the achievable data rates. Although it has been shown that biorthogonal TH-BPPM effectively doubles the data rate relative to the orthogonal TH-PPM [14], the inclusion of fast time hopping into the algorithm offsets this advantage. The data rates R_D for each N_H can be calculated using

$$R_D = \frac{k}{N_H \times T_o} \tag{3.3}$$

where $k = log_2(\text{number of symbols} M)$. For N_H = 1, 2 and 10, the associated data rates are 156.25, 78.125 and 15.625 Mbps, respectively.

The simulation workload is directly influenced by the total number of pulses transmitted (i.e., bits generated), the SNR (which determines E_b/N_o), the number of system transmitters (N_T), the number of multipath replications (N_{MP}) and the number of time hops per symbol (N_H). The total number of bits generated is not a predetermined simulation parameter; simulations continue until a C.I. of 95% is achieved with ±10% accuracy, i.e., until 300 errors accrue for given factors. The number of bits generated is used in calculations but does not influence the model. As E_b/N_o increases, the probability of a bit error decreases. This requires more iterations of the loops shown in Fig. 3.1 and increases system workload. The variations in system workload have no bearing on simulation outcomes.

3.6 Factors

For all simulations, the composite UWB signal is specified by a combination of signal power, multiple access, multipath, hops per communication symbol, network synchronization and user code.

3.6.1 Signal Power. The model is first validated against analytical results obtained from (3.5) over fixed average power E_b/N_o levels 0 to +10 dB in increments of 1.0 dB. These values provide estimated performance levels typically found in communication networks and are sufficient to characterize the biorthogonal TH-BPPM system performance with varying levels of N_H. The effects of multiple transmitters and multipath levels are studied using a fixed E_b/N_o that provides a P_b^H of 10^{-3}. This value is chosen to permit performance comparison with previously published results for orthogonal TH-PPM [27]. The E_b/N_o required at the demodulator input to meet the $P_b^H = 10^{-3}$ specification is dependent on N_H (*processing gain*). The E_b/N_o values (vertical dashed lines in Fig. 3.2) used for N_H = 1, 2, and 10 were 6.789, 3.7792 and -3.2105 dB, respectively. For all simulation results, the received power of *all* undesired interfering multiple access signals is identical to the received power of the desired signal.

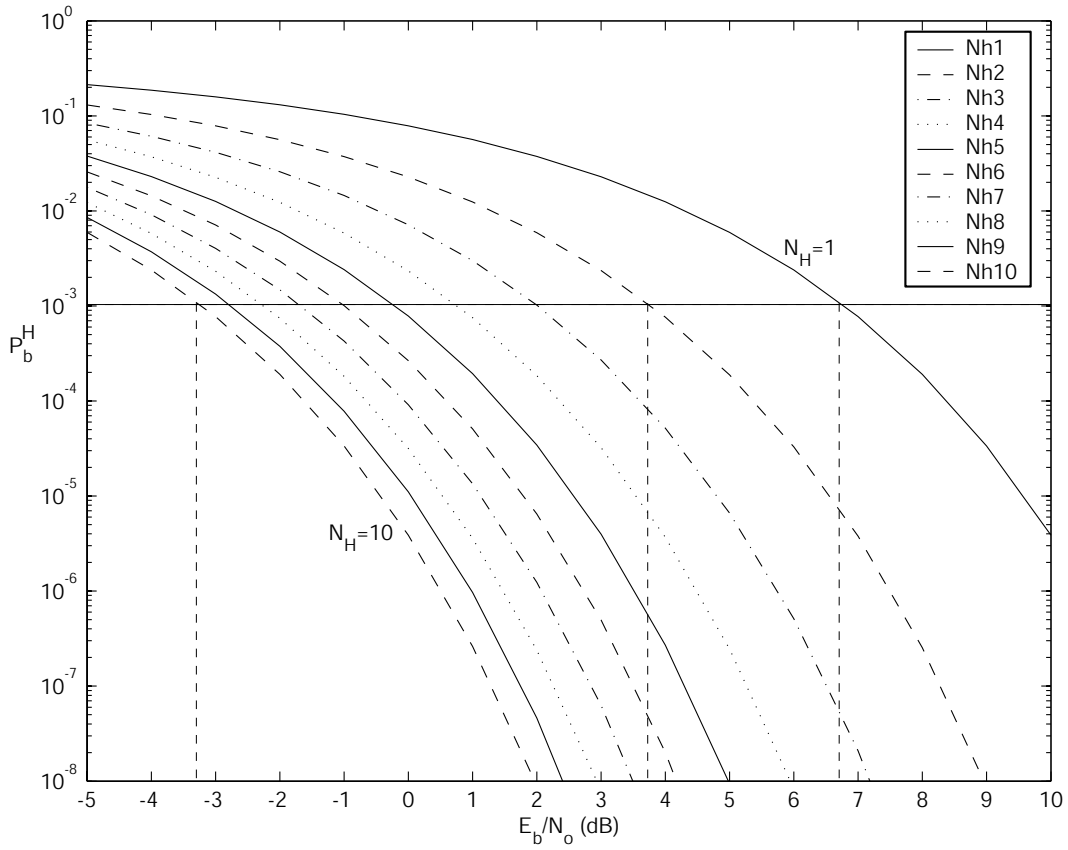

Figure 3.2: Analytical communication performance for fast time hopped systems (vertical dashed lines indicate E_b/N_o values for $P_b^H = 10^{-3}$ as indicated in Section 3.6.1)

3.6.2 Multiple Access. Using the E_b/N_o values established in Section 3.6.1, network communication performance is evaluated for N_T equal 1 to 15 transmitters (one desired and up to 14 multiple access interferers). As the number of transmitters increases, more collisions occur and destructive interference increases, increasing the expected BER. Simulation results will quantify BER changes due to added transmitters.

3.6.3 Multipath. Multipath interference (MPI) effects are characterized using an RMS time delay of 15.4 ns for each user's replicated signal [20]. The multipath remains constant over N_H pulses. In this manner, each message will observe the same realization of multipath. Data is generated at an E_b/N_o levels

for each N_H providing a BER of 10^{-3} as defined in Section 3.6.1 for five levels of multipath replication including $N_{MP} = 0,\ 5,\ 10,\ 20$ and 40 multipath replications per user. The two scenarios considered include: 1) a single transmit/receive link ($N_T = 1$) and 2) a network containing up to $N_T = 15$ transmitters.

3.6.4 Network Synchronization. For the communication link being evaluated, the transmitter of interest and receiver are perfectly synchronized. All other MA network signals arrive at the receiver either synchronously or asynchronously relative to the link being evaluated. For the asynchronous TH-BPPM cases considered, all interfering direct path MA signals are randomly time offset (delayed) in the range of $[0 : T_c]$. The asynchronous value remains constant for all direct and multipath signals from a given transmitter for the duration of the simulation. New realizations of the asynchronous offset are applied for each trial.

3.6.5 Fast Time Hopping. A fast time hopping technique is implemented whereby each symbol is replicated N_H times prior to coding and transmission. Fast time hopping effectively reduces the data rate by a factor of N_H. However, a processing gain of N_H is realized and BER improves due to the coherent detection process described in Section 3.7. The processing gains associated with large N_H values significantly impact simulation run time due to the number of symbols that would be generated to validate system performance. Therefore, N_H =1, 2, and 10 were used to generate varying workloads and represent low-level and high-level processing gains.

3.6.6 Code selection. System performance is highly dependent upon code choice since the success of the correlation receiver depends upon both the cross-correlation and auto-correlation characteristics of the codes used. In other words, the probability of bit error is affected by the number of signal collisions causing the receiver to incorrectly estimate a modulated signal. Since the various codes are used

to control pulse position and phase alignment, the choice of uniquely assigned user codes is a significant factor in MA and multipath communication performance.

Gold codes were chosen to implement multiple access coding to permit direct comparison with [2]. Gold codes are generated from 31-length m-sequences resulting in a family of 33, 31-length codes. The two "preferred pair" sequences originally used to develop the family of codes are discarded. The remaining 29 codes are reordered to set the particular user of interest and activation sequence for interfering transmitters. The reordering is based upon the the "zero-phase" cross correlation statistics of the m-sequences. "Zero-phase" refers to the fact that each code is cross correlated against all other codes just once. For a full characterization, the code of interest must be cross correlated against all other codes, shifted one bit and correlated again. This is repeated until each code of interest, in all phases, had been cross correlated against all other codes which makes it rather impractical.

The transmitter activation sequence used in all simulations (where the transmitter number relates to the row number of the original Gold code matrix) is

[21 1 7 13 19 4 5 12 15 29 9 23 11 22 24 25 28 2 10 20 27 3 14 18 17 6 8 26 16]

The particular coding $\{c_j\}$ sequence for the individual transmitter is calculated using the sliding window described in Section 2.3. Table 3.2 illustrates transmitter 21's Gold code sequence to chip offset sequence $\{c_j\}$ conversion using a sliding window of $r = 5$.

Table 3.2: Gold code sequence (top row) to chip offset sequence c_j (bottom row) conversion using a sliding window of $r = 5$ (Transmitter 21 illustrated)

1	1	1	1	1	1	1	0	0	1	1	1	0	0	1	0	0	1	1	0	0	1	1	1	0	1	1	1	1	0	0
31	31	31	30	28	25	19	07	14	28	25	18	04	09	19	06	12	25	19	07	14	29	27	23	15	30	28	25	19	07	15

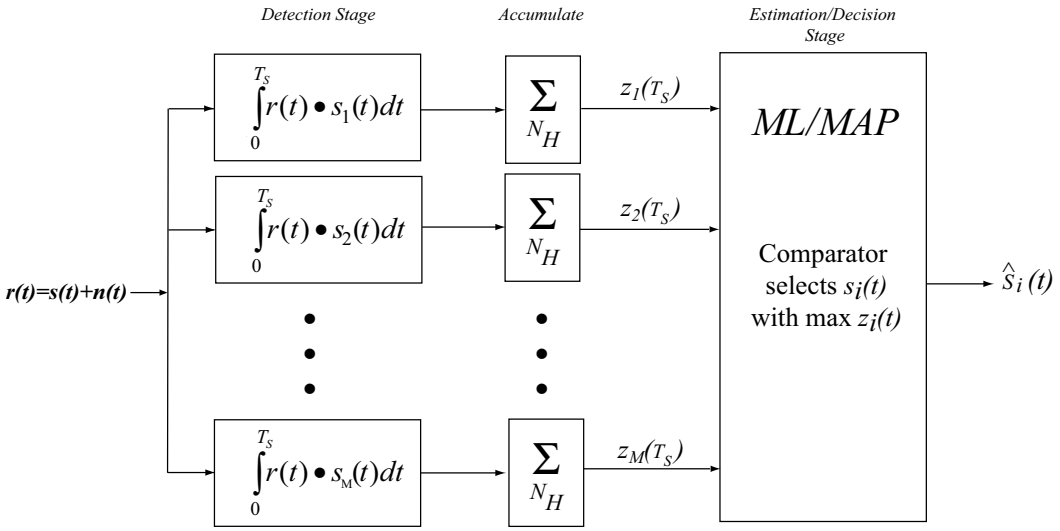

Figure 3.3: M-ary correlation receiver for maximum likelihood estimation of time hopped UWB waveforms

3.7 Evaluation Technique

UWB communication systems are in their infancy and have not yet proliferated to the extent where experimentation is easily done. Additionally, the TH-BPPM signaling evaluated in this study has not been fielded and is purely theoretical. Thus, simulation is the only practical means to investigate the biorthogonal TH-BPPM UWB communication technique. Additionally, simulation allows for quick modification of parameters to gather necessary data. Analysis is also greatly simplified.

Since the communication service involves properly transmitting data from one location to another, it is prudent to evaluate systems on their communication performance. The system modeled is a "fast time hopping" communication system whereby each symbol is generated, fast hopped/replicated N_H times, time hopped by applying the c_j code offset and transmitted. Using the multichannel correlation receiver of Fig. 3.3 under perfect "dehopping" conditions, *coherent detection* is achieved using a collection of cumulative decision variables, or test statistics $\{z_i\}$, as generated by accumulating N_H correlator outputs for each possible communication symbol $s_i(t)$ [28]. Assuming the signals are equally probable, maximum likelihood

(ML) estimation is achieved by estimating the symbol which corresponds to the Max $\{z_i\}$. It can be shown that the two processes used to generate test statistics in Fig. 3.4 are equivalent.

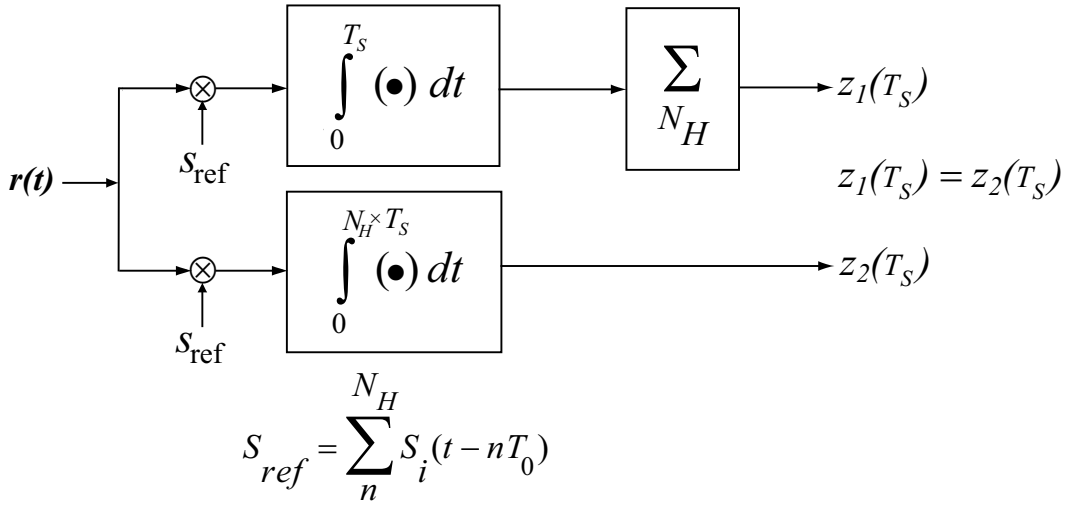

Figure 3.4: Detection stage correlator comparison

Performance optimization associated with binary antipodal signaling, i.e., maximum distance properties, directly translates to the biorthogonal symbol set. The biorthogonal symbol set generated by (2.4), as illustrated in Fig. 2.7, is equivalent to Gray coded quadrature PSK (QPSK) modulation where the theoretical bit error probability is given by

$$P_b = Q\left(\sqrt{\frac{2E_b}{N_o}}\right) \tag{3.4}$$

where Q is the complementary error function, E_b is the average received energy per bit, and $N_o/2$ is the two-sided noise power spectral density [28].

The generation of cumulative test statistics and selection of Max $\{z_i\}$ as shown in Fig. 3.3 provides equivalent estimation performance as a single channel system using N_H times the received energy [28]. Therefore, the improvement in communication performance as a result of hopping QPSK communication symbols N_H times, and coherently detecting at the receiver, results in theoretical bit error probability

P_b^H of

$$P_b^H = Q\left(\sqrt{N_H \cdot \frac{2E_b}{N_o}}\right). \tag{3.5}$$

For $N_H = 1$, the result is that expected of normal QPSK communication systems.

Equation 3.5 is analyzed to validate model results for the single user scenario and the results plotted against the analytical results shown in Fig. 3.2. Once the single user model is validated, the model is applied to multiple transmitters. Experimentation proceeds under the model's assumptions of AWGN with non-selective channel fading.

3.8 Workload

The simulation workload SNR and number of transmitters N_T allows direct comparison with [2]. These factors affect operation throughout the system. The total number of pulses generated, the noise through the channel, and the ability of the receiver to detect and estimate data symbols are all directly impacted. Providing the simulation with 10 SNR values and then 15 transmitter levels, 5 values for multipath replications, and 2 synchronization scenarios is consistent with published literature and reasonable given the memory and CPU speed of the computers available.

By using a fixed E_b/N_o as described in Section 3.6.1 and varying the four parameters N_T, N_{MP}, N_H and synchronization, a full factorial (4500 of 4500 potential workloads) is used to span the range of biorthogonal TH-BPPM UWB signals.

Table 3.3 outlines the multiple workloads submitted to the simulation with $N_H \in \{1, 2, 10\}$, $N_{MP} \in \{0, 5, 10, 20, 40\}$, $N_T = 1$ or 1 through 15, for both synchronous and asynchronous networks.

Table 3.3: Simulation Configurations

			Number of Hops (N_H)					
			1		2		10	
			Number of Transmitters (N_T)					
			1	1-15	1	1-15	1	1-15
Number of Multipath (N_{MP})	0	Sync	X	X	X	X	X	X
		Async		X		X		X
	5	Sync		X		X		X
		Async		X		X		X
	10	Sync		X		X		X
		Async		X		X		X
	20	Sync		X		X		X
		Async		X		X		X
	40	Sync		X		X		X
		Async		X		X		X

3.9 Experimental Design

The research is conducted using simulation in two phases. Initial results are used to validate the simulation model and verify values to be used in subsequent simulations. The second phase conducts the experiments.

This research characterizes bit error performance (P_b) of TH-BPPM multiple access schemes for UWB communications by first validating communication performance. This is done by varying the E_b/N_o, energy per bit divided by Additive White Gaussian Noise (AWGN) power spectral density, which proportionally maps to Signal-to-Noise Ratio (SNR). The ratio of incorrectly estimated bits to total number of bits received is used to calculate P_b^H. The simulated results are compared to analytic expectations obtained from (3.5). The number of hops per communication symbol (N_H) is fixed at one to validate the model against expected QPSK modulation results. Communication performance under interference conditions of Multiple Access Interference (MAI), Multipath Interference (MPI), and varied levels of N_H

are simulated to study the robustness of UWB communication systems operating in a network of users with realistic propagation delays.

Analysis of TH-BPPM begins with development of components used in a UWB communication system. The system is tested by introducing AWGN into the channel to validate the model. Various noise power values are used to test the multiple access TH method. Finally, a specific E_b/N_o is chosen to validate against previous results and serve as an appropriate power level for digital communications. Biorthogonal TH-BPPM communication performance, in terms of BER, is reported for increasing levels. MAI, MPI, and N_H are introduced into each scheme and performance results analyzed for both synchronous and asynchronous network operation.

This research assesses the performance characteristics of a UWB communication system operating at a center frequency of 5.0 GHz. Though the trends reported should hold for any operating frequency, the parameters are fixed as described in Section 3.5 to indicate simulated performance in the unlicensed spectrum as authorized by the FCC for UWB systems.

Experimentation occurs in several phases. Initially, the benchmark of 300 bit errors is reduced to develop the code and gain a coarse understanding of the effect SNR has on the results. Once the code is fully developed, the model is validated. SNR is varied over 10 values, mapping to E_b/N_o values between 0 and 10 dB, in increments of 1.0 dB. Following validation of $N_H = 1$ results with expected theoretical performance described by (3.4), experimentation proceeds to incorporate multiple transmitters.

The number of total transmitters (including the transmitted signal of interest plus all interfering transmitters) is varied from $N_T = 1$ to 15 transmitters. The SNR is fixed at E_b/N_o levels of Section 3.6.1. All trials are recorded for a synchronous network of users. These trials are repeated for users transmitting asynchronously.

MPI is added by creating $N_{MP} = 0,\ 2,\ 5,\ 10$ and 40 multipath reflections per user and recording the synchronous and asynchronous results for a fixed SNR.

Fast time hopping is implemented by replicating each symbol N_H times, encoding and transmitting with various levels of MAI and MPI for synchronous and asynchronous networks.

Figure 3.1 flow charts the logic behind the $Matlab^{®}$ algorithm. An $N_T \times 200$ matrix of random data streams is generated to insure independence among transmitters. The **time hopping** is easily implemented by replicating every k-bits of every user/transmitter; in this manner each k-bits are undergo the same modulation and TH coding processes prior to "transmission". The 4-ary UWB **modulator** merely maps k-bits to one of four discretely sampled and stored UWB TH-BPPM waveforms. The **asynchronous** values represent the random activation of the transmitters. Once activated, the transmitter remains activated for the duration of the simulation and the $(0 : T_C)$ pulse offset value unique to each transmitter remains constant and is applied to every pulse from that transmitter.

Additive white gaussian noise (AWGN) is applied to each pulse. The noise realizations for $N_T \cdot (N_{MP} + 1)$ discrete waveforms are generated once per iteration of the 200-bit loop to maintain independence among individual transmitters, yet preserve the small time correlation among pulses from a single transmitter. The stored noise values are retrieved and applied as required for a given user, symbol, mulipath link. The composite signal (signal of interest + interferers) is applied to the input of the 4-channel correlator. The correlator creates test statistics Z_i that are accumulated N_H times. The accumulator sums the test statistics and sends the values to the maximum likelihood estimator. The largest summed Z_i value is chosen and mapped to the appropriate data bits. Once all data bits for a given iteration are collected, they are compared to the original data bits. The number of errors are accumulated and the entire process is repeated until 300 errors are generated to provide the confidence interval described in Section 3.4.

3.10 Analyze and Interpret Results

Successful results must support the goals of this research to determine, for particular error levels, the E_b/N_o required and multiple access interference experienced when using spreading codes for fast time hopping. P_b is plotted versus E_b/N_o for various multiple access codes. Fixing the value of E_b/N_o, P_b is plotted versus the number of transmitters given the levels of multipath and number of hops per symbol. Results are anticipated to follow a logarithmic scale between 0.5 and 10^{-6} for P_b over the range of E_b/N_o values. Similar results are expected when P_b is plotted over the range of user levels. The values of P_b are distinguishable at various factor levels so that only visual tests are needed to determine uniqueness, avoiding the need for a t-test [26] to determine statistically unique values. Previous analysis of variance (ANOVA) [2] quantified the real-time impact of code, number of transmitters, and multipath levels on system performance in terms of impact on the P_b. From the ANOVA results in [2], the significant factors affecting the output value P_b are determined to be equivalent given the similarity in signal structure.

Similar to the *BER Improvement* in [17] for code improvements, the significant factor effects are quantified by determining the average *BER Improvement* (over 15 transmitters) for increasing N_H values relative to a $N_H = 1$ baseline. Since a ratio can be determined for the P_b value of one N_H relative to that of another code, a decibel value is used to report the BER improvement. The average ratio of P_b values is calculated for the 15 transmitters. From this improvement factor, the performance of each hopping level can be assessed.

3.11 Summary of Experimental Setup

This chapter outlines the methodology used to assess the performance of a "fast time hopping," multiple access, UWB communication system using TH-BPPM modulation. The transmitter, receiver, channel, and multiple interferers are modeled to provide assess communication performance with specific emphasis on the multiple

access and modulation components. Since the system's service is transmitting data bits, the metrics used to characterize system performance are probability of bit error versus E_b/N_o and size of the network in terms of transmitters.

A two stage simulation process provides the basis for the research. Initial simulations are validated against accepted analytical performance equations. Once the model is verified, the parameters are adjusted for the actual experimentation.

Analysis of the results compares the relative effects of E_b/N_o, number of transmitters, number of multipaths, number of time hops per symbol, and network synchronization. Results are expected to provide accurate indicators of how the factors affect communication performance using the TH-BPPM modulation scheme. Additional insight into the trade-offs between time-hopping, data rate, and fast time hopping should be extracted.

IV. Results and Analysis

4.1 Single Channel Communication Performance

A single communication link TH-BPPM model with $N_H = 1$ was validated against analytic bit error given by (3.5). Figure 4.1 compares the simulation results against the analytic bit error curve and previously reported orthogonal TH-PPM performance [2]. For the $N_H = 1$ case, the biorthogonal TH-BPPM provided performance gains equivalent to that of Gray-coded QPSK; improved performance at a given E_b/N_o and an effective doubling of the data rate.

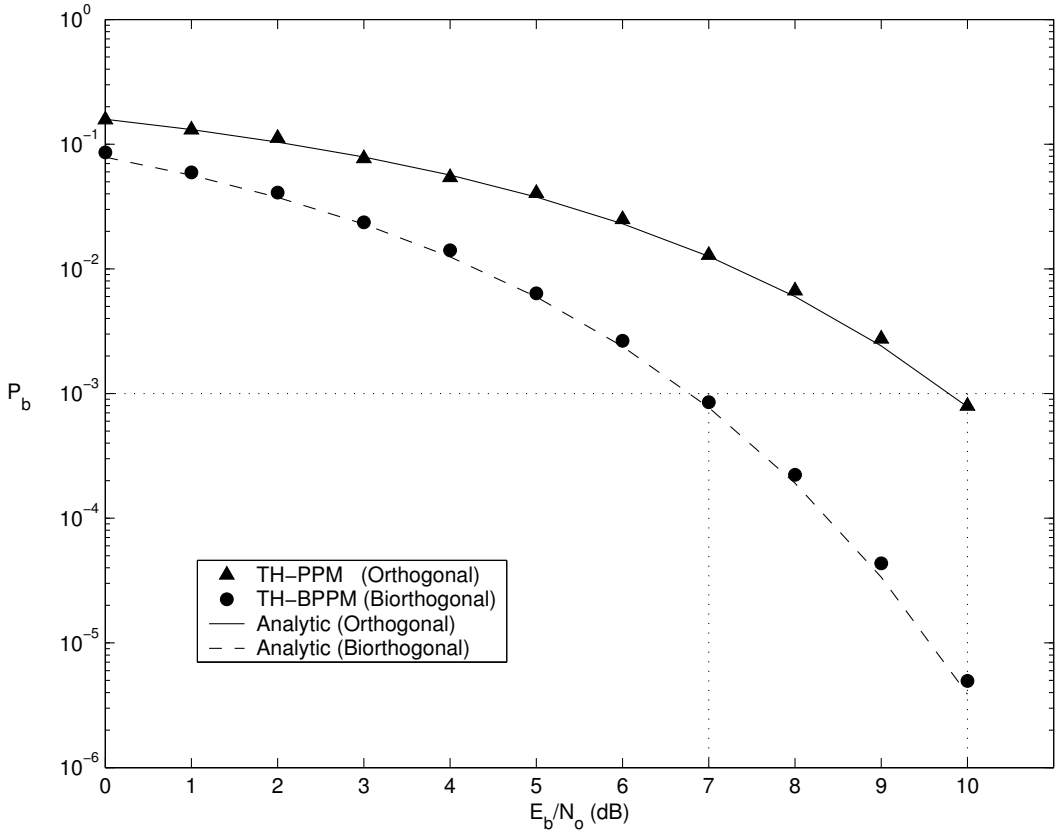

Figure 4.1: Single Channel Communication Performance: orthogonal TH-PPM and biorthogonal TH-BPPM with no hopping ($N_H = 1$)

Once validated for $N_H = 1$, the model was extended to $N_H = 2$, 3, and 4 cases where simulated P_b^H results shown in Fig. 4.2 remain consistent with analytic

results of (3.5) and Fig. 3.2. As a single communication channel, the TH coding does not have any effect on measured performance. For each simulation, a random binary data stream was produced and k bits mapped to a communication symbol. Each symbol is then hopped N_H times (time modulated), transmitted, and received. Symbols were detected using a 4-channel correlator which sums N_H test statistics $\left(\hat{Z}_i\right)$ to estimate each symbol $\left(\hat{S}_i\right)$. The $\left(\hat{S}_i\right)$ are mapped back to bits and the estimated data bits are compared to the original data bits and the total number of errors recorded. Using the 300 bit error criteria, data in Fig. 4.3 produces median values for mean squared error and standard deviation between simulated and analytic results of 3.7×10^6 and 1.4×10^3, respectively. The impact of fast time hopping each communication symbol is inherent *processing gain* in BER performance is evident. Improved bit error rates are achievable at lower E_b/N_o levels. As shown in Fig. 4.2, for a given bit error rate (P_b) there is a reduction in required E_b/N_o to achieve that P_b as N_H increases. Alternately stated, for a given E_b/N_o value, P_b decreases (improves) as N_H increases; the trade off for this improved performance is a $1/N_H$ reduction in effective data rate.

4.2 Network Communication Performance, N_H=1

Network performance for biorthogonal TH-BPPM was first compared to that of orthogonal TH-PPM. Using fixed average power to achieve desired communication performance of $P_b = 10^{-3}$, i.e., $E_b/N_o \approx 9.78$ dB for orthogonal TH-PPM and $E_b/N_o = 6.789$ dB for biorthogonal TH-BPPM, network communication performance is evaluated for 1 to 15 transmitting users (one desired and up to 14 multiple access interferers). For all simulation results, the received power of all undesired interfering multiple access signals is identical to the received power of the desired signal.

4.2.1 Multiple Access Interference Effects. Initial MA performance characterization was done using $N_H = 1$ to isolate code selection and assignment effects in the absence of fast time hopping processing gain present. Using fixed average power

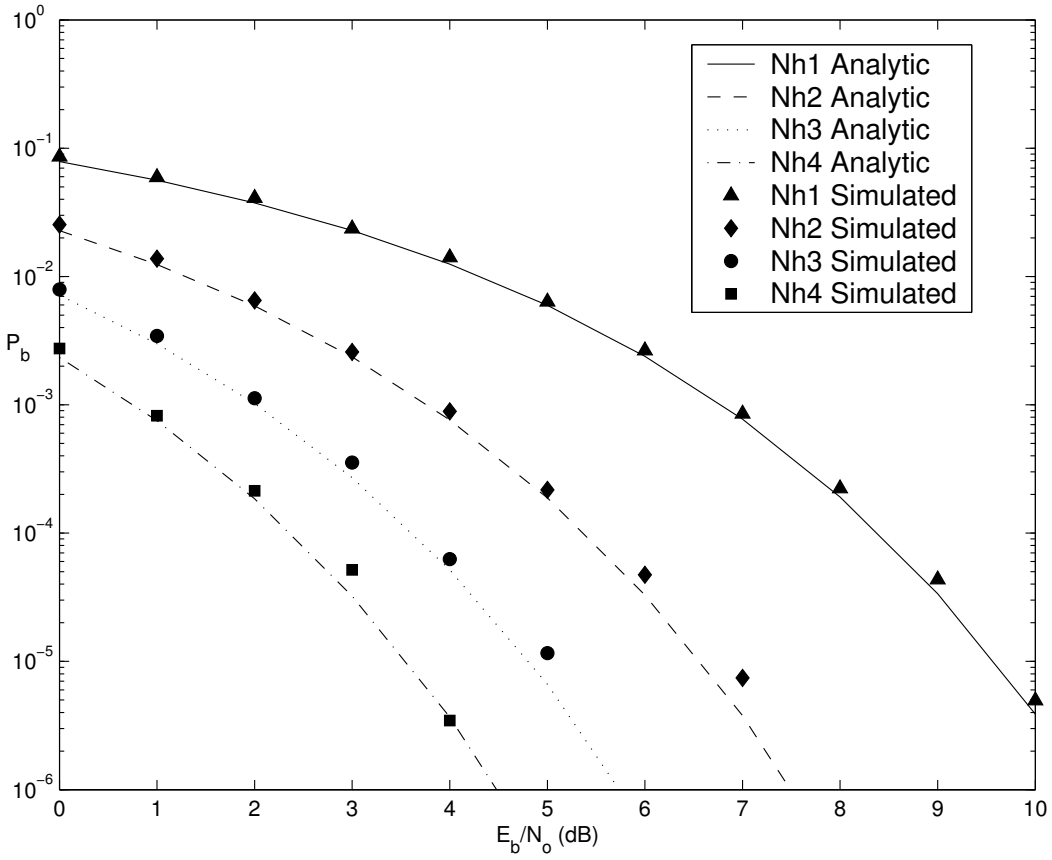

Figure 4.2: Single Channel Communication Performance: Biorthogonal TH-BPPM using $N_H = 1,\ 2,\ 3$ and 4 hops per communication symbol

to achieve desired communication performance of $P_b = 10^{-3}$, i.e., $E_b/N_o = 6.789$ dB for biorthogonal TH-BPPM, multiple access performance is evaluated using $N_H = 1$ for a network containing up to $N_T = 15$ transmitters. In this case, the receiver under test receives one desired signal and $(N_T - 1)$ undesired, direct path multiple access interferers. For all simulation results, the received power of *all* undesired interfering multiple access signals is identical to the received power of the desired signal. The receiver under test is perfectly synchronized to the transmitter of interest while all other signals are received either synchronously or asynchronously. For the asynchronous network, all multiple access interferers are randomly offset (delayed) in time over $[0, T_c]$.

Network multiple access results for biorthogonal TH-BPPM were generated for comparison with orthogonal TH-PPM results of [27]. Simulation results are shown in Fig. 4.3 for the *synchronous* (filled symbols) and *asynchronous* (unfilled symbols) networks. This filled and unfilled symbol convention is maintained throughout the document.

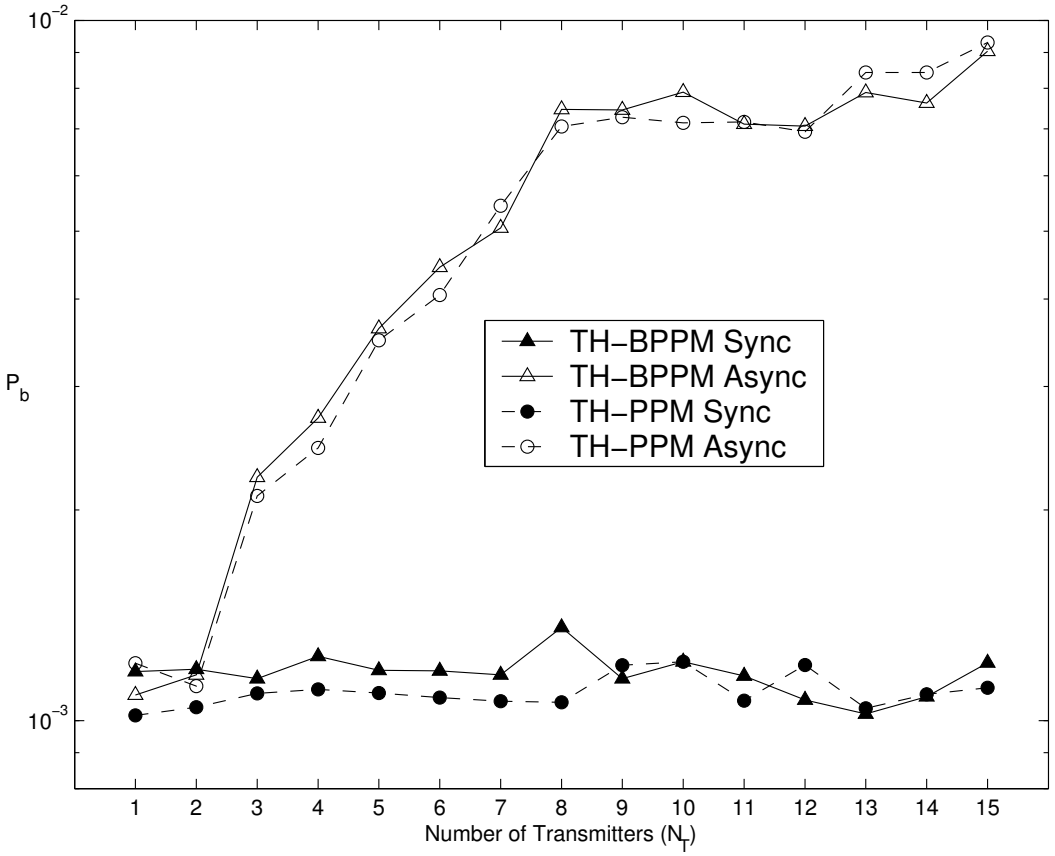

Figure 4.3: Multiple Access Performance: Asynchronous and Synchronous Networks using Orthogonal TH-PPM [15] and Biorthogonal TH-BPPM with Gold Coding

As in previous orthogonal TH-PPM work [17], the synchronous biorthogonal TH-BPPM network experiences minimal symbol collisions with Gold code assignment and bit error performance is virtually unaffected by variation in N_T. The "jump" occurring in both TH-BPPM asynchronous networks when the eighth transmitter joins the network is not due to premature termination of the Monte Carlo

simulation process. Rather, the "jump" is due to specific Gold code assignment and ordering. The particular collection of Gold codes used for generating Fig. 4.3 results (15 of 31 possible codes are assigned to transmitters) is such that the cross-correlation response between the joining eighth transmitter and previous seven transmitters destructively interferes (degrades P_b). Reassigning this particular collection of codes, or randomly reassigning a new collection of 15 codes from the original 31, yields results consistent with those in Fig. 4.3 but with the anomalous "jump" occurring at a different N_T value. Figure 4.4 shows the effect of altering the transmitter activation sequence (reassignment of the original collection) and how the "jump" now occurs when the fifth transmitter joins the network. To permit comparison with subsequent results, the original Gold code collection and assignment used for generating Fig. 4.3 results is maintained throughout all simulations.

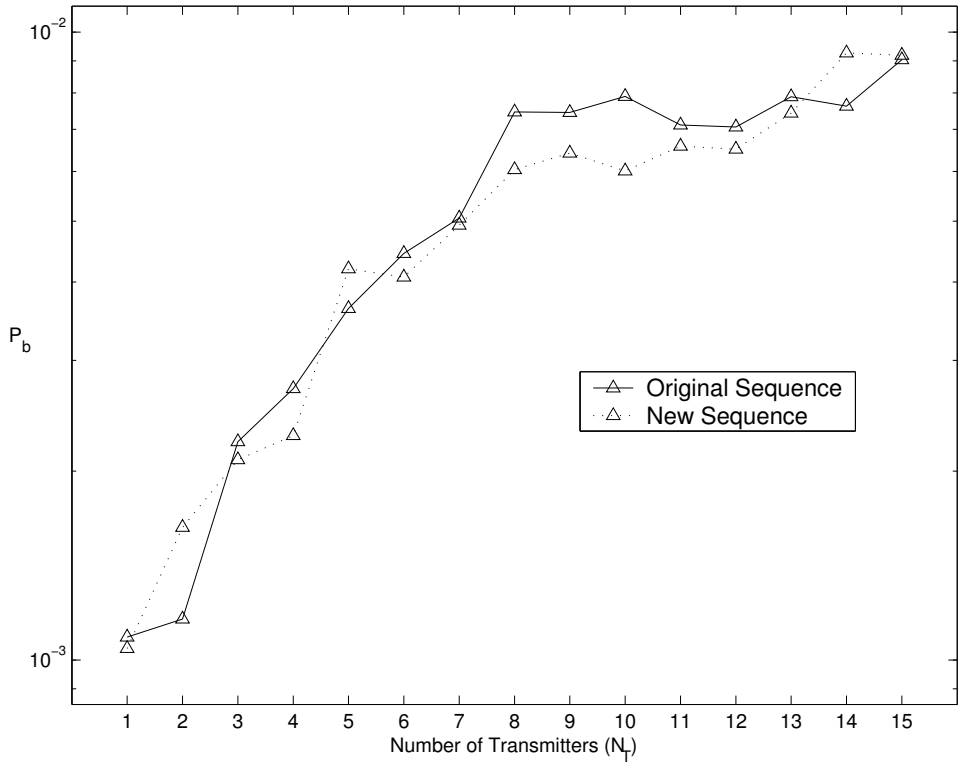

Figure 4.4: Network Multiple Access Performance: Synchronous TH-BPPM "jump" shift due to Gold code sequence assignment

Using a *BER improvement* metric, i.e., the average ratio (over all 15 transmitters) of synchronous P_b performance to asynchronous P_b performance, results in Fig. 4.5 indicate a synchronized network containing up to $N_T = 15$ transmitters yields an average *BER improvement* of approximately -6.30 dB with orthogonal TH-PPM and approximately -5.9 dB with biorthogonal TH-BPPM; nearly equivalent performance is indicated for both techniques.

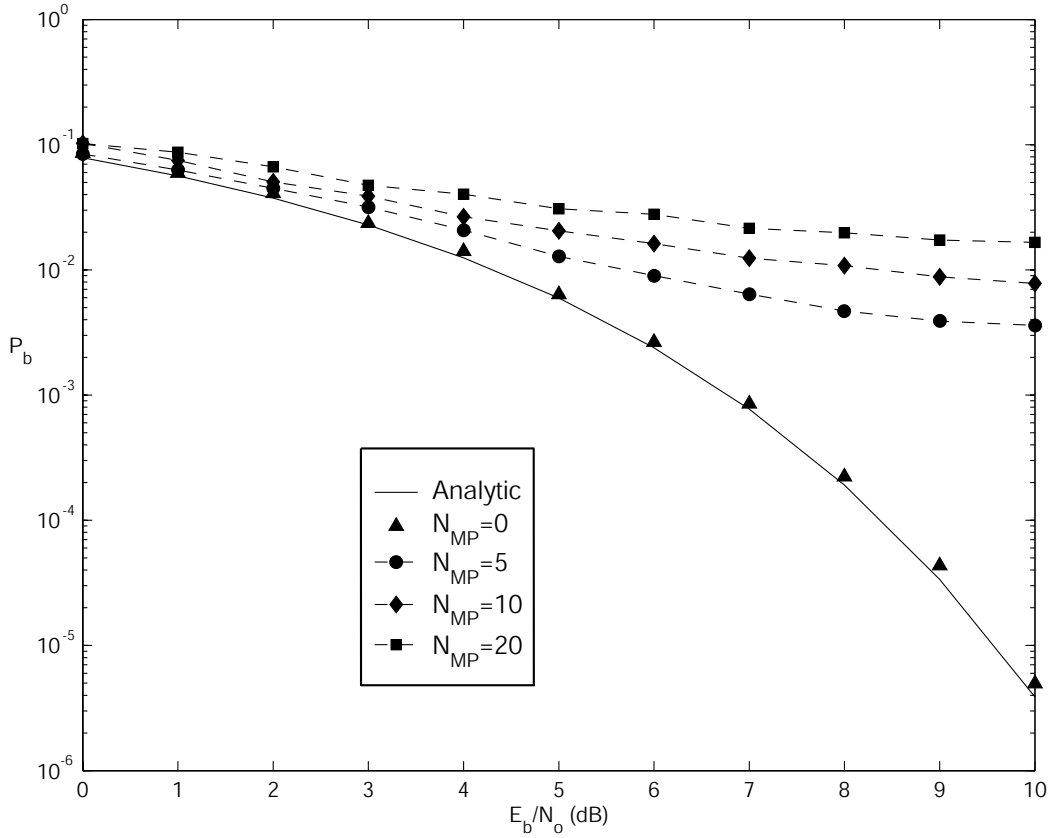

Figure 4.5: Single channel communication performance with N_{MP} multipath replications present

4.2.2 Multipath Interference Effects. Figure 4.5 shows multipath interference effects on a single channel communication system for $N_{MP} = 0,\ 5,\ 10$, and 20 multipath replications. The degradation of BER is evident throughout the range of E_b/N_o considered. At lower E_b/N_o levels, thermal/channel noise dominates and

determines performance. As the E_b/N_o increases the multipath interference dominates and overshadows noise effects in establishing system performance. The trends in Fig. 4.5 indicate that doubling N_{MP} reduces BER by approximately 3.6 dB. For $E_b/N_o = 10$, the *simulated performance/analytic results* for $N_{MP} = 5,\ 10,\ 20$ is approximately $-29.4,\ -33.01$, and -33.76 dB, respectively.

For the remainder of the simulated results presented in this chapter, Fig. 4.6 through Fig. 4.11, the labeling convention of Table 4.1 is used.

Table 4.1: Labeling Convention for Fig. 4.6 through Fig. 4.11

Time Hopping	Network Synchronization	Figure Position
$N_H = 1$ (Solid Line & $\triangle$)	*Synchronous* (Filled)	*Synchronous* (Upper Left)
$N_H = 2$ (Dashed Line & $\bigcirc$)	*Asynchronous* (Unfilled)	*Asynchronous* (Upper Right)
$N_H = 10$ (Dotted Line & $\diamondsuit$)		*Combined* (Lower Middle)

Figure 4.6 provides performance results for $N_H = 1$ synchronous and asynchronous networks with $N_{MP} = 0,\ 5,\ 10,\ 20,\ 40$. For all multipath levels, the composite received waveform consists of $N_T \times (N_{MP} + 1)$ total signals, including one direct *desired* signal, $(N_T - 1)$ direct multiple access *interfering* signals and $N_T \times N_{MP}$ delayed multipath *interfering* signals. Whenever multipath is present $(N_{MP} > 0)$, statistically equivalent results are achieved under simulated multipath conditions independent of synchronization. The results exhibit the expected performance degradation as N_T and N_{MP} increase; most notably, synchronized network advantages which are apparent in the $N_{MP} = 0$ case quickly diminish when multipath interference is introduced.

4.3 Network Communication Performance, $N_H > 1$

4.3.1 Time Hopped MA Performance. Network MA performance was characterized with processing gain present using symbol repeat values of $N_H = 2$ and 10. In these cases, the average *received* symbol power was fixed to achieve desired theoretical communication performance of $P_b = 10^{-3}$. For the $N_H = 2$ and 10

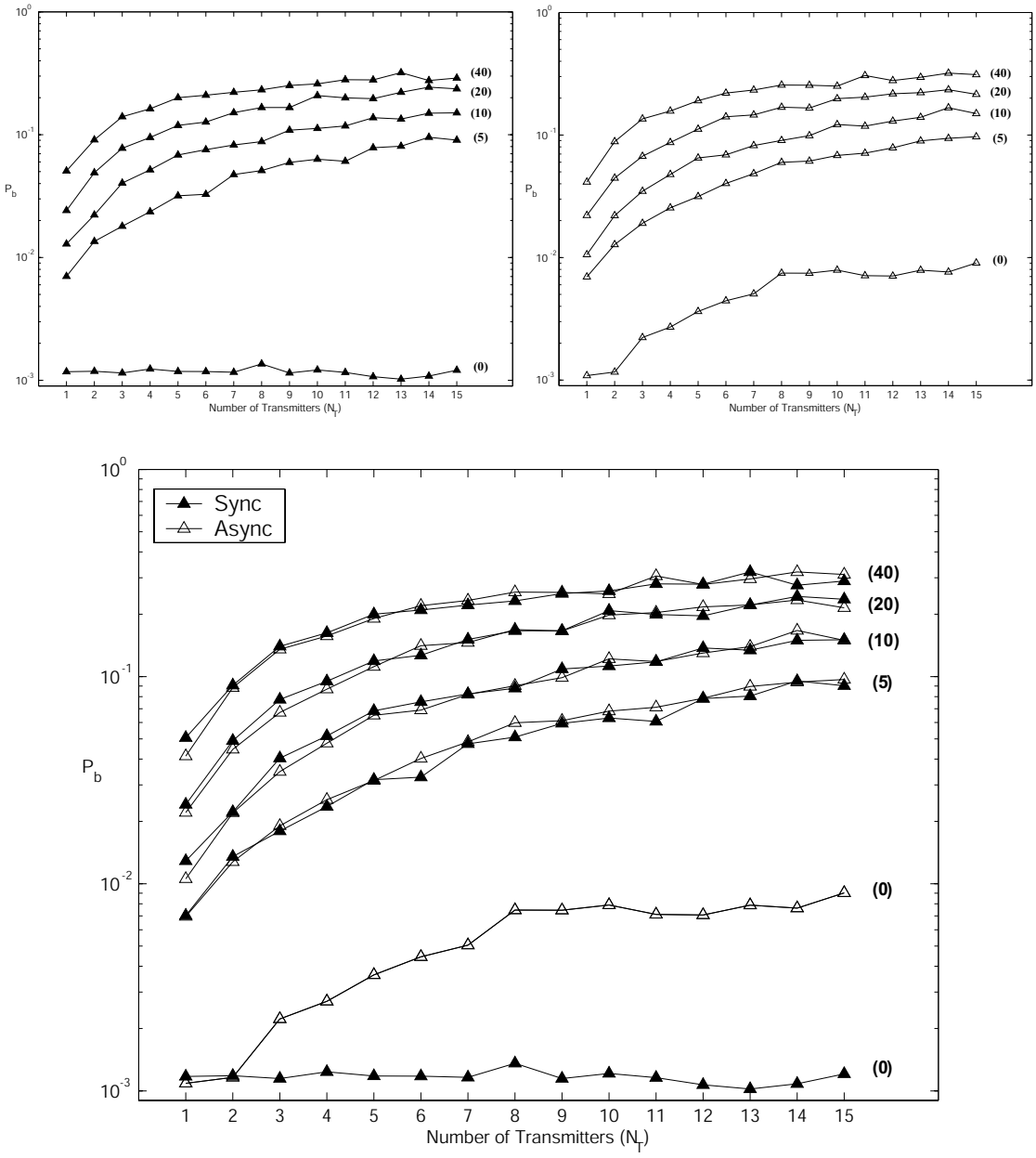

Figure 4.6: Network multipath interference effects for $N_H = 1$ using $N_{MP} = 0,\ 5,\ 10,\ 20$ and 40 replications (indicated in parenthesis)

cases, the received $E_b/N_o = 6.789$ ($N_H = 1$ $E_b/N_o value$) $- 10Log_2(N_H)$ dB which is approximately 3.78 and -3.21 dB, respectively. Multiple access performance was evaluated for a network containing up to $N_T = 15$ transmitters. As in the $N_H = 1$ case, the receiver under test receives one desired signal and $(N_T - 1)$ undesired, di-

rect path multiple access interferers. The received power of *all* undesired interfering multiple access signals was set equal to the desired signal power and perfect synchronization is assumed for the signal of interest. All other signals are received either synchronously or asynchronously. Results presented in Fig. 4.7 show network performance improvement due to processing gain, a function of the repeating symbols. As indicated, symbol hopping has minimal impact on synchronous network performance because of the unique code assignments. For the asynchronous network all multiple access interferers are randomly offset (delayed) in time over $[0, T_c]$. As expected, network performance degrades as transmitters are added to the network and the number of collisions between symbols increases. However, for the asynchronous network a 6-fold and 8-fold P_b^H improvement is indicated for $N_T = 15$ using $N_H = 2$ and $N_H = 10$, respectively.

4.3.2 Time Hopped MA Performance with Multipath Present. Multipath interference (MPI) effects were characterized using an RMS time delay value of 15.4 ns for each transmitter's replicated signal [20]. Data was generated using E_b/N_o values as defined in Section 4.3.1 for various multipath replications (N_{MP}), including $N_{MP} = 0,\ 5,\ 10,\ 20$ and 40 reflections per transmitter. Figures 4.8, 4.9, and 4.10 show network communication performance for $N_T = 1$ to 15 transmitters with $N_{MP} = 5,\ 10$, and 20, respectively. Figure 4.11 is a composite of all multipath results. Fast time hopping improves bit error performance for all cases where $N_{MP} < N_H$. As implemented in the algorithm, all benefits of time hopping are diminished once the level of multipath equals or exceeds the number of hops. For example, the performance improvement for $N_H = 10$ shown in Figure 4.8 is no longer present in Fig. 4.9. Similar results have been obtained for $N_H = 20$.

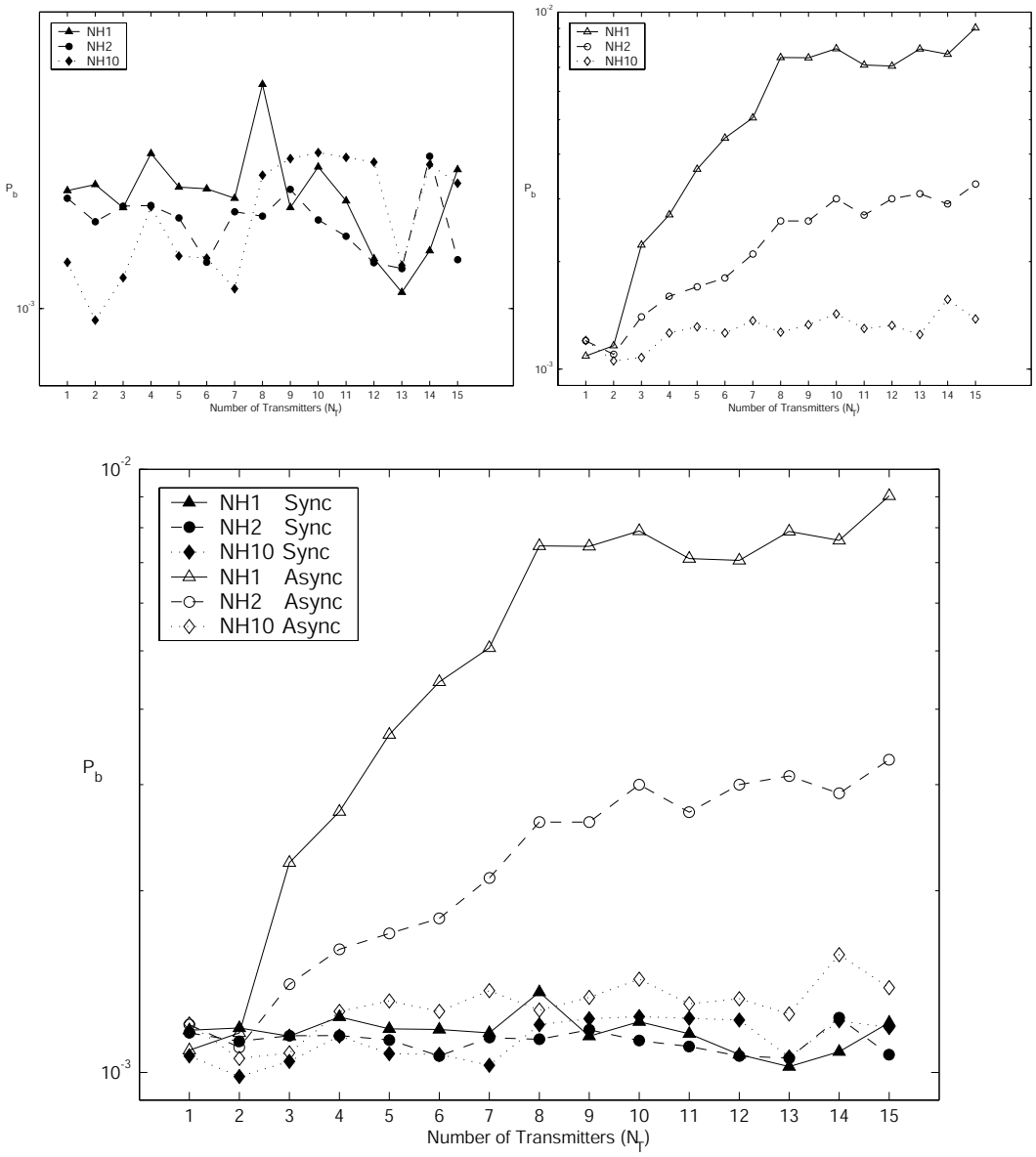

Figure 4.7: Network multiple access performance *with processing gain* of $N_H = 1,\ 2,\ 10$ and no multipath present ($N_{MP} = 0$)

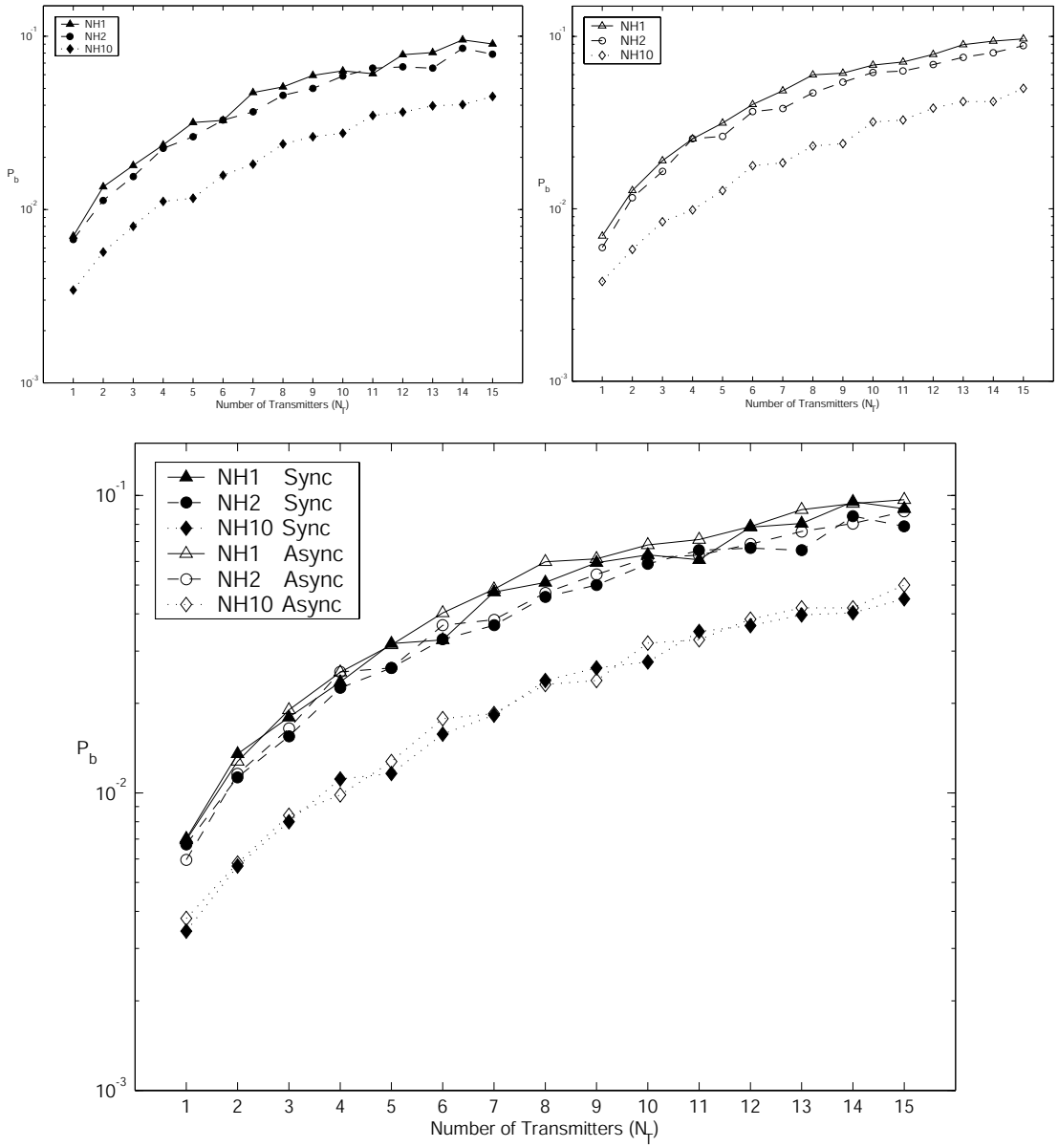

Figure 4.8: Network Communication Performance with Time Hopping ($N_{MP} = 5$ multipath replications per transmitter present)

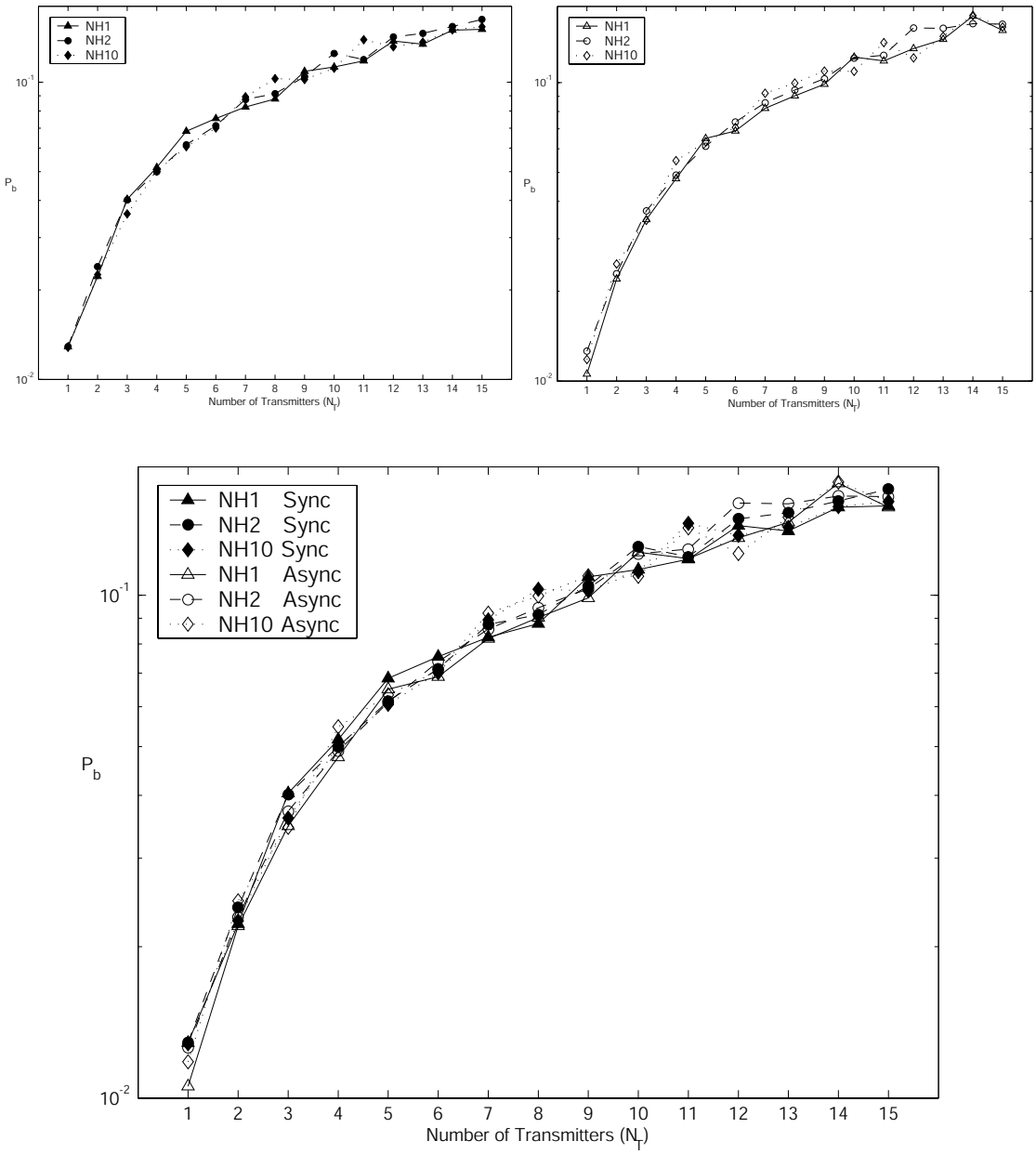

Figure 4.9: Network Communication Performance with Time Hopping ($N_{MP} = 10$ multipath replications per transmitter present)

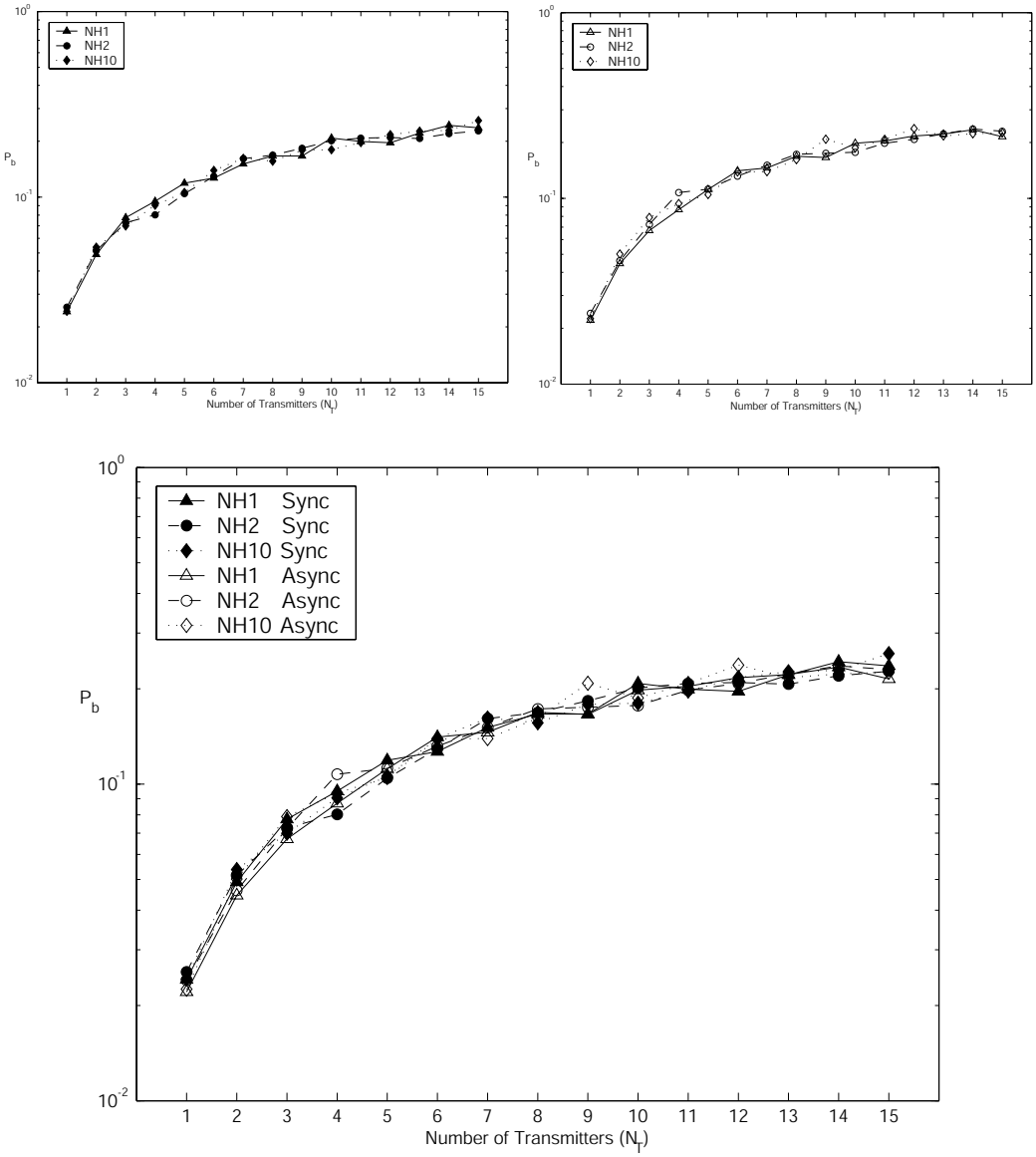

Figure 4.10: Network Communication Performance with Time Hopping ($N_{MP} = 20$ multipath replications per transmitter present)

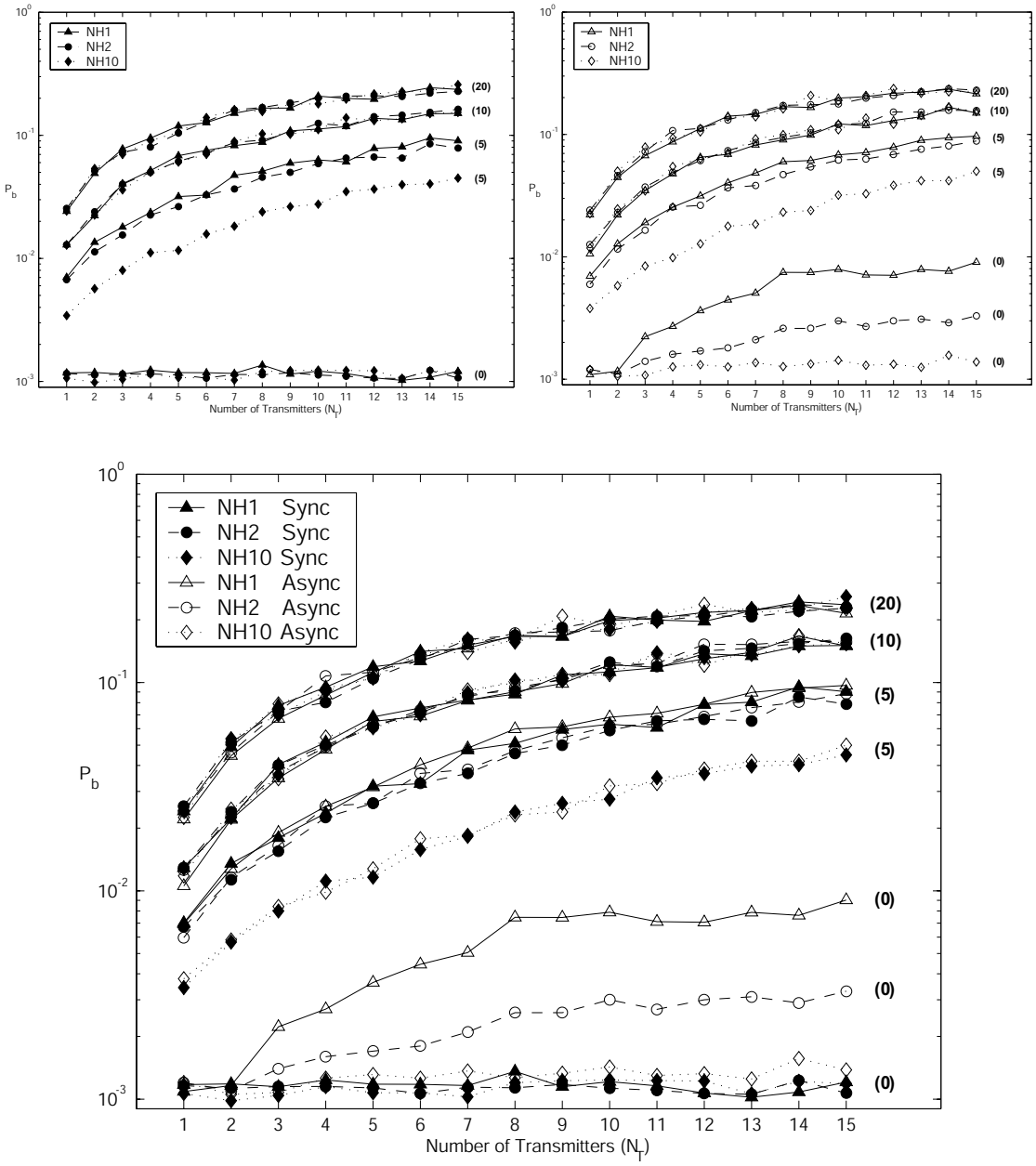

Figure 4.11: Network Communication Performance with Time Hopping ($N_{MP} = 0$, 5 10, and 20 multipath replications per transmitter present)

Table 4.2 shows average BER improvement provided by fast time hopping as compared to the $N_H = 1$ case. In this case, the BER improvement is given by

$$BER\ Improvement = 10 \times log_{10}\left(\frac{Average\ BER\ of\ N_T = 1\ to\ 15}{Average\ BER\ of\ N_H\ =\ 1}\right) \qquad (4.1)$$

where the average BER performance of $N_H = 1$ synchronous or asynchronous is designated as the baseline performance, as appropriate. The more negative the decibel number reported, the greater the improvement provided by fast time hopping relative to $N_H = 1$ for the multipath level reported. For example, in a synchronized network containing up to 15 transmitters, TH-BPPM modulation with $N_H = 10$ provides approximately -5.9 dB at $N_{MP} = 0$ and approximately -3.6 dB at $N_{MP} = 5$. At $N_{MP} = 10$ the BER rates for the hopped and $N_H = 1$ cases are not statistically different.

The BER improvement numbers in Table 4.2 and Table 4.3 indicate how time hopping advantages diminish as N_{MP} becomes greater than N_H.

Table 4.2: Time Hopping BER Improvement (dB) of (4.1)

	$N_H = 2$		$N_H = 10$	
N_{MP}	Sync	Async	Sync	Async
0	-0.162162	-3.537399	-0.118594	-5.901617
5	-0.53014	-0.583243	-3.441116	-3.596834
10	0.084626	0.171558	$\approx 10^{-5}$	0.177112
20	-0.078261	0.0852	-0.003777	0.139703
40	-0.099825	-0.053802	0.097463	-0.110156

Table 4.3 reports the BER improvement between synchronous and asynchronous performance for fast time hopping at various N_{MP} levels. The BER improvement in this case is the ratio of synchronous performance to asynchronous perfor-

mance for each N_H value and is given by

$$BER\ Improvement(x) = 10 \times log_{10}\left(\frac{BER_{Sync},\ N_T = 1\ to\ 15,\ N_H = x}{BER_{Async},\ N_T = 1\ to\ 15,\ N_H = x}\right) \quad (4.2)$$

where the average asynchronous BER performance (BER_{Async}) of the particular N_H level is designated as the baseline performance. Again, the more negative the decibel number reported, the greater the synchronized performance is relative to the asynchronous network for a given N_H value. For example, in a network containing up to 15 transmitters, the BER improvement factor for TH-BPPM modulation with $N_H = 10$ varies from approximately -0.57 to 0.14 which indicates minimal variation between synchronous and asynchronous network performance. At $N_{MP} = 10$ the BER rates for the hopped and $N_H = 1$ cases are not statistically different. As expected, the $N_H = 1$ case has a greater variation but as multipath is added any benefits from synchronous operation are lost.

Table 4.3: Synchronous BER Improvement (dB) of (4.2)

N_{MP}	$N_H = 1$	$N_H = 2$	$N_H = 10$
0	-6.713958	-3.049962	-0.572538
5	-0.284994	-0.205711	-0.155646
10	0.019582	-0.034833	-0.036261
20	0.070459	-0.031231	-0.017065
40	-0.101052	-0.094326	0.139463

V. Conclusions

5.1 Research Contributions

Multiple access performance is characterized for UWB waveforms using biorthogonal TH-BPPM with pseudorandom coding. Fast time hopping is introduced and bit error expressions derived for biorthogonal TH-BPPM signaling. Results expand upon the binary TH-PPM work of [27] regarding Gold code time hopping sequences. TH-BPPM multiple access network performance is compared head-to-head with published results for an orthogonal TH-PPM technique. Contributions to the UWB research knowledge base include UWB communication, multiple access interference (MAI), multipath interference (MPI), and fast time hopping performance characterization using 31-length Gold codes over both synchronous and asynchronous networks.

5.2 Summary of Findings

5.2.1 Findings Without Fast Time Hopping ($N_H = 1$). A single communication channel using biorthogonal TH-BPPM model produced median values for mean squared error and standard deviation between simulated and analytic results of 3.7×10^6 and 1.4×10^3, respectively. For the $N_H = 1$ case, the biorthogonal TH-BPPM provided performance gains equivalent to that of Gray-coded QPSK; improved bit error performance at a given E_b/N_o and an effective doubling of the data rate. Using fixed average power to achieve desired communication performance, the synchronous biorthogonal TH-BPPM network experiences minimal symbol collisions with Gold code assignment and bit error performance is virtually unaffected by variation in N_T. A *BER improvement* metric is introduced to quantify performance gains relative to the $N_H = 1$ asynchronous results. Results indicate a synchronized network containing up to $N_T = 15$ transmitters yields an average *BER improvement* of approximately -6.30 dB with orthogonal TH-PPM and approximately

-5.9 dB with biorthogonal TH-BPPM; nearly equivalent performance is indicated for both techniques. Multipath interference on a single communication channel degrades BER throughout the range of E_b/N_o considered. At lower E_b/N_o levels, thermal/channel noise dominates and determines performance. As E_b/N_o increases the multipath interference dominates and overshadows noise effects in establishing system performance. The observed trends indicate that doubling N_{MP} reduces BER by approximately 3.6 dB. For $E_b/N_o = 10$ dB, the *simulated performance-to-analytic results* ratio for $N_{MP} = 5,\ 10,\ 20$ replications is approximately $-29.4,\ -33.01$, and -33.76 dB, respectively. In a multiple access environment containing multipath, performance results that are not statistically different are achieved under simulated multipath conditions independent of synchronization. The results exhibit the expected performance degradation as N_T and N_{MP} increase; most notably, synchronized network advantages which are apparent in the $N_{MP} = 0$ case quickly diminish when multipath interference is introduced.

5.2.2 Findings With Fast Time Hopping. Fast time hopping each communication symbol improves BER performance. For a given E_b/N_o value, bit error rate P_b decreases (improves) as N_H increases; the trade-off for this improved performance is a $1/N_H$ reduction in effective data rate. Fast time hopping, i.e., $N_H = 2$ and 10 cases, show network performance improvement due to processing gain. Fast time hopping symbols has minimal impact on synchronous network performance because of the unique code assignments. However, for the asynchronous network a 6-fold and 8-fold P_b^H improvement is indicated for $N_T = 15$ using $N_H = 2$ and $N_H = 10$, respectively. Fast time hopping improves bit error performance for all cases where $N_{MP} < N_H$. Average BER improvement provided by fast time hopping is compared to the $N_H = 1$ case. In a synchronized network containing up to $N_T = 15$ transmitters, TH-BPPM modulation using $N_H = 10$ provides approximately -5.9 dB improvement at $N_{MP} = 0$ and approximately -3.6 dB improvement at $N_{MP} = 5$. At $N_{MP} = 10$, the BER rates for the hopped and $N_H = 1$ cases are not statistically

different. BER improvement between synchronous and asynchronous performance for fast time hopping is shown for various N_{MP} levels. In a network containing up to $N_T = 15$ transmitters, the BER improvement factor for TH-BPPM modulation with $N_H = 10$ hops varies from approximately -0.57 to 0.14 (minimal variation between synchronous and asynchronous network performance). At $N_{MP} = 10$ the BER rates for the hopped and $N_H = 1$ cases are not statistically different. As expected, the $N_H = 1$ case has a greater variation but as multipath is added any benefits from synchronous operation are lost. The BER improvement statistics show time hopping advantages diminish as N_{MP} becomes greater than N_H.

5.3 Future Research

5.3.1 Error Correction with M-Ary Signaling. The fast time hopping scheme implemented provides results consistent with coherent pulse integration techniques without potential advantages of error correction capabilities. The hop encoding process could be thought of as a (N_H, 1) block encoder operating at the symbol level. A mapping sequence for the received signals could be developed and implemented in the estimation stage. Simulation results could be validated against known block encoder message error and bit error expressions of [28] given as

$$P_M = \sum_{j=t+1}^{N_H} \binom{n}{k} \left(P_b^H\right)^j \left(1 - P_b^H\right)^{N_H - j}, \text{ and} \tag{5.1}$$

$$P_b = \frac{1}{N_H} \sum_{j=t+1}^{N_H} j \binom{n}{k} \left(P_b^H\right)^j \left(1 - P_b^H\right)^{N_H - j} \tag{5.2}$$

where t is equal to the error correcting capability of the code.

5.3.2 Code Selection. Thirty-one length Gold codes were used to provide multiple access capability while minimizing collisions between users. The processing gain inherent in fast time hopping showed significant gains and should be evaluated against other codes of varying lengths, such as the random and Gold-127 reported

in [2] to characterize code type effects. The degradation responses reported in [17] may be lessened by employing fast time hopping.

5.3.3 Channel Models. The UWB model provided equal energy signals for all multiple users and multipath replications in a AWGN channel. Although this is a worst case analysis, it may not necessarily reflect real-world phenomenology. The model may be improved by considering the TH-PPM multiuser characterization research of [29]. No fading channel effects were implemented and all multipath signals were received with equal power. Rayleigh, log-normal, or Markov($\Delta - k$) could be applied to the waveforms to more accurately predict system performance.

5.3.4 Pulse Repetition Modifications. Fixed symbol rates were used for all simulations. Pulse generation schemes that allow overlapping pulses, i.e., chip intervals less than two times the symbol duration, would increase the overall throughput. The simulation data rates were fixed, but varying the data rate based on symbol overlap conditions may impact communication performance. An effort could be undertaken to determine optimal pulse spacing and chip interval to maximize efficiency and avoid overspreading effects described in [2]. The time hopping code development algorithm could be tested to determine optimal register size and resultant time hop c_j values.

5.3.5 Interference Testing. Potential interference issues are commonplace in UWB discussions given the UWB signal characteristics described in Section 1.2. Characterization of UWB waveform interference effects on military applications, e.g., Global Positioning System, radar systems, aircraft avionics, and wireless communications should be undertaken. Facilities and resources exist within the military test community to efficiently and effectively conduct susceptibility modeling, simulation and testing.

5.3.6 UWB Hardware Evaluation. The TH-BPPM modulation scheme has not yet been fielded. Investigation into possible implementation techniques may be warranted given the performance gains demonstrated via modeling and simulation.

Bibliography

1. M. J. Copps and K. J. Martin, "First report and order," Federal Communications Commission, Washington, D.C. 20554, report FCC 02-48, April 2002.
2. C. M. Canadeo, "Ultra wide band multiple access performance using th-ppm and ds-bpsk modulations," Master's thesis, Air Force Institute of Technology, 2950 Hobson Way, Wright-Patterson AFB, OH, March 2003.
3. J. McCorkle and M. Rofheart, "Report to the federal communications commission on rules regarding ultra-wideband transmission systems," XtremeSpectrum Inc., 1077 30th Street NW, suite 311, Washington, DC 20007, Fall 1998.
4. M. I. Skolnik, *Introduction to Radar Systems*, 3rd ed. 1221 Avenue of the Americas, New York, NY 10020: McGraw-Hill, Inc., 2001.
5. D. R. McKinstry and R. M. Buehrer, "Issues in the performance and covertness of uwb communications systems," in *The 2002 45th Midwest Symposium on Circuits and Systems*, vol. 3. Blacksburg, VA, USA: Virgina Tech, Aug 2002, pp. 601–604.
6. C. Fowler, J. Entzminger, and J. Corum, "Assessment of ultra-wideband technology," Defense Advanced Research Projects Agency, Arlington, VA, 22209-2308, contract DAAH-88-C-0131, November 1990.
7. J. Aurand, *Measurement Of Short Pulse Propagation Through Concrete Walls*, ser. Ultra-Wideband Short Pulse Electromagnetics. New York: Plenum Press, 1997.
8. R. J. Fontana, "On range-bandwidth per joule for ultra wideband and spread spectrum waveforms, Multispectral Solutions, INC.," July 2000.
9. Q. Hua, J. Shin, S. Sung, , and W. Teng, "The role of ultra wideband in wireless home networks," Conference Paper, University of Colorado, Boulder, December 1992.
10. "First report and order: Revision of part 15 of the commission's rules regarding ultra-wideband transmission systems," Washington, Report Series ET Docket 98-153, Apr. 2002.
11. G. F. Ross, "Transmission and reception system for generating and receiving base-band duration pulse signals without distortion for short base-band pulse communication system," Patent, 1973.
12. J. D. Taylor, *Introduction to Ultra-Wideband Radar Systems*. 27 Congress Street, Salem, MA 01970: CRC Press, Inc., 1995.
13. B. Sklar, *Digital Communications*. New Jersey: Prentice Hall, 2001.

14. D. J. Clabaugh, M. A. Temple, R. A. Raines, and C. M. Canadeo, "Uwb multiple access performance using time hopped pulse position modulation with biorthogonal signaling," *IEEE Conference on UWB Systems and Technologies (UWBST 2003)*, November 2003.

15. D. J. Clabaugh, M. A. Temple, R. A. Raines, R. O. Baldwin, and J. P. Stephens, "Uwb biorthogonal ppm in a time hopped synchronous network with multipath present," *The 8th World Multi-Conference on Systemics, Cybernetics and Informatics (SCI 2004)*, March 2004.

16. R. Scholtz, "Multiple access with time-hopping impulse modulation," *Proceedings of 1993 IEEE Military Communications Conference (MILCOM 2003), Boston MA*, vol. 2, pp. 447–450, October 1993.

17. C. M. Canadeo, M. A. Temple, R. O. Baldwin, and R. A. Raines, "Code selection for enhancing uwb multiple access communication performance using th-ppm and ds-bpsk modulations," *IEEE Wireless Communications and Networking Conference (WCNC 2003)*, vol. 1, pp. 678–682, March 2003.

18. D. Sarwate and M. B. Pursley, "Crosscorrelation properties of pseudorandom and related sequences," *Proceedings of the IEEE*, vol. 68, pp. 593–619, May 1980.

19. P. Misra and P. Enge, *Global Positioning System Signals, Measurements, and Performance*. P.O. Box 692, Lincoln, Massachusetts 01773: Ganga-Jamuna Press, 2001.

20. J. R. Foerster, "The performance of a direct-sequence spread spectrum ultra-wideband system in the presence of multipath, narrowband, interference, and multiuser interference," May 2002.

21. F. Zhu, Z. Wu, and C. R. Nassar, "Generalized fading channel model with application to uwb," *IEEE Conference on UWB Systems and Technologies (UWBST 2002)*, November 2002.

22. K. Siwiak and A. Petroff, "A path link model for ultra wide band pulse transmissions," Time Domain Corporation, Huntsville AL, Tech. Rep.

23. D. Cassioli, M. Z. Win, and A. F. Molisch, "A statistical model for the uwb indoor channel," Rhodes, Greece," Conference Proceedings of the IEEE VTC-2001, May 2001.

24. J. R. Foerster, "The effects of multipath interference on the performance of uwb systems in an indoor wireless channel," May 2001.

25. M. Z. Win and R. A. Scholtz, "On the robustness of ultra-wide bandwidth signals in dense multipath environments," *IEEE Communications Letters*, vol. 2, no. 2, Feb. 1998.

26. R. Jain, *The Art of Computer Systems Performance Analysis*. New York: John Wiley & Sons, Inc., 1991.

27. C. M. Canadeo, M. A. Temple, R. O. Baldwin, and R. A. Raines, "Uwb multiple access performance in synchronous and asynchronous networks," *IEE Electronics Letters*, vol. 39, pp. 880–882, January 2003.

28. J. G. Proakis, *Digital Communications*, 4th ed., G. T. Hoffman and J. M. Morris, Eds. New York, New York: McGraw-Hill, 2001.

29. G. Durisi, "On the validity of gaussian approximation to characterize the multiuser capacity of uwb th ppm," May 2002.

REPORT DOCUMENTATION PAGE

Form Approved
OMB No. 074-0188

1. REPORT DATE *(DD-MM-YYYY)*	2. REPORT TYPE	3. DATES COVERED *(From – To)*
23-03-2004	Master's Thesis	Oct 2003 – Mar 2004

4. TITLE AND SUBTITLE
CHARACTERIZATION OF ULTRA WIDE BAND MULTIPLE ACCESS PERFORMANCE USING TIME HOPPED-BIORTHOGONAL PULSE POSITION MODULATION

5a. CONTRACT NUMBER

5b. GRANT NUMBER

5c. PROGRAM ELEMENT NUMBER

6. AUTHOR(S)

Clabaugh, Donald J., CMSgt, USAF

5d. PROJECT NUMBER

5e. TASK NUMBER

5f. WORK UNIT NUMBER

7. PERFORMING ORGANIZATION NAMES(S) AND ADDRESS(S)

Air Force Institute of Technology
Graduate School of Engineering and Management (AFIT/EN)
2950 Hobson Way, Building 640
WPAFB OH 45433-7765

8. PERFORMING ORGANIZATION REPORT NUMBER

AFIT/GE/ENG/04-03

9. SPONSORING/MONITORING AGENCY NAME(S) AND ADDRESS(ES)

AFRL/SNRW
Mr. James P. Stephens
2241 Avionics Circle Rm N2L3
WPAFB OH 45433-7333 (937) 255-5579 x4239
james.stephens@wpafb.mil

10. SPONSOR/MONITOR'S ACRONYM(S)

11. SPONSOR/MONITOR'S REPORT NUMBER(S)

12. DISTRIBUTION/AVAILABILITY STATEMENT

APPROVED FOR PUBLIC RELEASE; DISTRIBUTION UNLIMITED

13. SUPPLEMENTARY NOTES

14. ABSTRACT

The FCC's release of its UWB First Report and Order in April 2002 spawned renewed interest in impulse signaling research. This work combines Time Hopped (TH) multiple access coding with 4-ary UWB Biorthogonal Pulse Position Modulation (TH-BPPM). Multiple access performance is evaluated in a multipath environment for both synchronous and asynchronous networks. Fast time hopping is implemented by replicating and hopping each TH-BPPM symbol N_H times. Bit error expressions are derived for biorthogonal TH-BPPM signaling and results compared with previous orthogonal TH-PPM work. Without fast time hopping ($N_H = 1$), the biorthogonal TH-BPPM technique provided gains equivalent to Gray-coded QPSK; improved BER at a given E_b/N_o and an effective doubling of the data rate. A synchronized network containing up to $N_T = 15$ transmitters yields an average *BER improvement* (relative to an asynchronous network) of approximately -6.30 dB with orthogonal TH-PPM and approximately -5.9 dB with biorthogonal TH-BPPM. Simulation results indicate that doubling the number of multipath replications (N_{MP}) reduces BER by approximately 3.6 dB. Network performance degrades as N_T and N_{MP} increase and synchronized network advantages apparent in the $N_{MP} = 0$ case diminish with multipath interference present. With fast time hopping ($N_H > 1$) improves BER performance whenever $N_{MP} < N_H$ while reducing effective data rate by $1/N_H$. Compared to the $N_H = 1$ synchronized network, TH-BPPM modulation using $N_H = 10$ provides approximately -5.9 dB improvement at $N_{MP} = 0$ and approximately -3.6 dB im provement at $N_{MP} = 5$. At $N_{MP} = 10$, the BER for the hopped and $N_H = 1$ cases are not statistically different; with $N_H = 10$ hops, *BER improvement* varies from approximately -0.57 to 0.14 dB (minimal variation between synchronous and asynchronous network performance).

15. SUBJECT TERMS

Ultra Wideband, UWB, TH-BPPM, Biorthogonal, Pulse Position Modulation, Multiple Access, Interference, Multipath Transmission, Fast Time Hopping

16. SECURITY CLASSIFICATION OF:			17. LIMITATION OF ABSTRACT	18. NUMBER OF PAGES	19a. NAME OF RESPONSIBLE PERSON
REPORT	ABSTRACT	c. THIS PAGE			Dr. Michael A. Temple, AFIT/ENG
U	U	U	UU	78	19b. TELEPHONE NUMBER *(Include area code)* (937) 255-6565, ext 4279; e-mail: michael.temple@afit.edu